AD-A099 567 MICHIGAN UNIV ANN ARBOR GAS DYNAMICS LABS F/G 20/4
THE EFFECT OF CROSS FLOW AND ISOLATED ROUGHNESS ELEMENTS ON THE--ETC(U
JAN 77 W W WILLMARTH, L K SHARMA, S INGLIS N00014-76-C-0571
UNCLASSIFIED UM-014439-01 NL

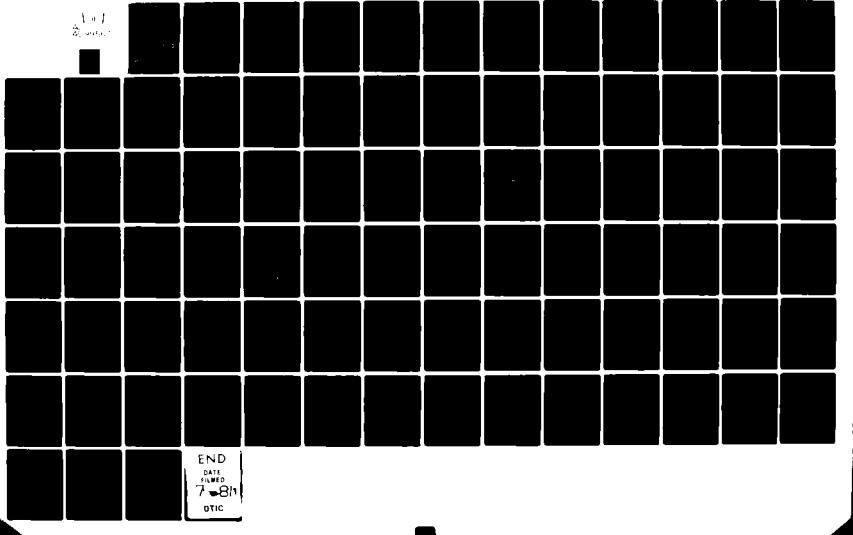

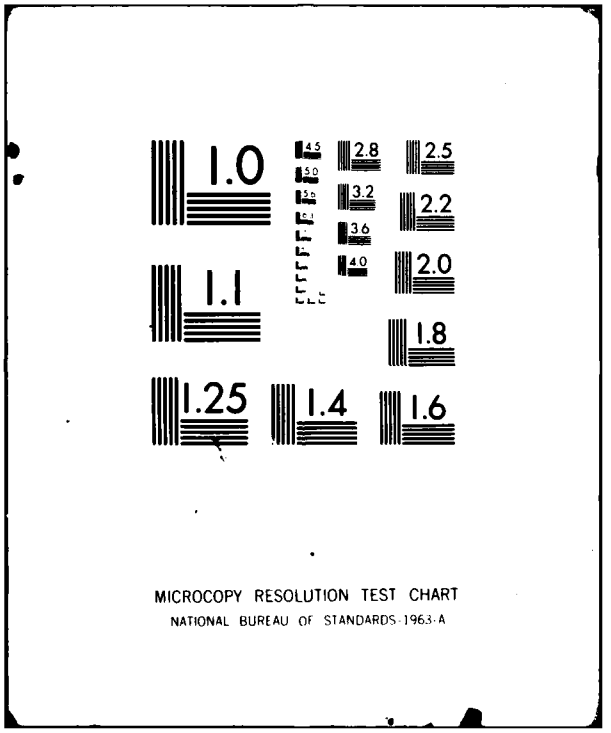
1.0
1.1
1.25
1.4
1.6
1.8
2.0
2.2
2.5
2.8
3.2
3.6
4.0
4.5
5.0
5.6
MICROCOPY RESOLUTION TEST CHART
NATIONAL BUREAU OF STANDARDS-1963-A

014439-01

The Effect of Cross Flow and Isolated Roughness Elements on the Boundary Layer and Wall Pressure Fluctuations on Circular Cylinders

WILLIAM W. WILLMARTH
Principal Investigator
LALIT K. SHARMA
SCOTT INGLIS

January 1977

Department of the Navy
Office of Naval Research
Contract No. N00014-76-C-0571
Washington, D. C.

Department of Aerospace Engineering
Gas Dynamics Laboratories

(14) ANN-014439-01

(6)

THE EFFECT OF CROSS FLOW AND ISOLATED ROUGHNESS ELEMENTS ON THE BOUNDARY LAYER AND WALL PRESSURE FLUCTUATIONS ON CIRCULAR CYLINDERS

(10) William W. Willmarth
Principal Investigator

Lalit K. Sharma
Scott Inglis

(12) 85

(11) January 1977

(15) N00014-76-C-0571

Department of the Navy
Office of Naval Research
Contract No.N 00014-76-C-0571
Washington, D.C.

Department of Aerospace Engineering
The University of Michigan

401 757

ABSTRACT

In this paper pressure fluctuation measurements on smooth cylinders aligned with the flow have been extended to include the effect of slight cross flow and isolated roughness elements. A yaw angle of a few degrees is sufficient to produce severe asymmetry of the outer portion of the boundary layer as deduced from impact pressure measurements using computer controlled traversing gear. The root-mean-square surface pressure fluctuations are a maximum on the windward surface but only slightly larger than with no yaw. On the leeward surface they are much lower. The power spectrum of the pressure has greater energy density at high frequencies on the windward surface and at low frequencies on the leeward side. With no cross flow the root-mean-square surface pressure is greatly increased by a cylindrical collar placed around the cylinder. A collar which increases the diameter by 50% more than doubles the wall pressure three diameters downstream. The spectra of the pressure scale with collar thickness and the intensity of the surface pressure fluctuations scales with the ratio of collar thickness to distance downstream.

TABLE OF CONTENTS

1. INTRODUCTION

In two previous papers, Willmarth and Yang (1970) and Willmarth et al. (1976), detailed studies are reported of the boundary layer profiles and wall pressure fluctuations developed on long circular cylinders aligned with the flow. In the course of setting up the flow fields for these investigations of the axially symmetric boundary layer on cylinders, it was discovered that a very small angle of yaw was sufficient to cause gross asymmetry of the boundary layer. For example, measurements of the boundary layer of the order of 7.5 meters from the nose of a 7.62 cm diameter cylinder showed serious asymmetry of the velocity profiles for flow misalignments of the order of 0.05 degrees.

In an actual flow that is approximately parallel to the axis of a long circular cylinder (for example an arrow, lance, or towing cable and the like) the cylinder surface is rarely perfectly smooth nor is the cylinder axis a straight line. Owing to free stream turbulence or other disturbances in the flow misalignments of the order of a few degrees can easily occur. The present investigation was undertaken in order to evaluate the effect of flow misalignment and surface roughness on the turbulent boundary layer flow field and wall pressure fluctuations. There do not appear to be any detailed measurements of the turbulent boundary layer profiles on rough or slightly yawed cylinders. However, Reid and Wilson (1963) have considered the problem of the drag of rough cylinders. They report calculations of the drag based on the friction coefficient of rough walled pipe flow and

measurements of the drag of stranded towing cables. In order to learn more about the nature and severity of the effect of yaw and roughness on the boundary layer flow on long cylinders an exploratory investigation on a cylinder of 25.4 mm diameter was undertaken.

2. EXPERIMENTAL EQUIPMENT AND APPARATUS

A. WIND TUNNEL AND CYLINDRICAL MODEL

The experiments were carried out in a specially constructed vertical wind tunnel with an octagonal test section 30.48 cm wide and 5.5 meters long. The facility was used in a previous investigation and is described in Willmarth et al. (1976). The flow in the empty tunnel is uniform and parallel within a few percent. The 25.4 mm circular cylinder model was also used in our previous work, Willmarth et al. (1976). It was made from segments of aluminum tubing with accurately machined joints held together by an internal steel cable in tension.

Three cylindrical collars 1.59 mm, 3.18 mm and 6.35 mm thick and 50.8 mm long were used to test the effect of isolated roughness elements on the wall pressure fluctuations. The collars were split in half and clamped on the cylinder with a flat steel spring around the circumference of the collar and inset flush with the surface. The collars were easily positioned at any station on the cylinder. Figure 3 contains a sketch of the 6.35 mm thick collar.

B. INSTRUMENTATION FOR MEASUREMENTS OF THE MEAN FLOW FIELD

Approximate measurements of the mean flow field about the yawed cylinder were made using an impact pressure tube. The impact tube was constructed from a 5 cm straight length of 0.812 mm diameter stainless steel hypodermic tubing. The

inside diameter of the tubing was 0.457 mm. The end of the tube was cut off at right angles to the axis and all burrs were carefully removed. The impact tube was supported by a larger diameter tube inserted through a slot cut in the side of the tunnel and fitted with a flexible rubber seal. The impact pressure tube was mounted on a traversing mechanism driven by two stepping motors and could be positioned at any point near the yawed cylinder under the control of a digital minicomputer. The impact pressure was used to compute the approximate fluid velocity assuming the validity of Bernoulli's law and that the static pressure at any point was constant and equal to the free stream static pressure.

The computer controlled traversing gear was actuated by two sigma model 18-1408 D40-F stepping motors with 50:1 gear ratio that were controlled by a 16 bit Computer Automation, Alpha 16 minicomputer with 8K words of memory. The interface between the minicomputer and stepping motors was constructed in our laboratory. The computer software was designed to traverse the impact pressure probe along any continuous path about the yawed cylinder. The path was specified by the cartesian coordinates of the points along the path at which the impact pressure was measured. At each measuring point the computer driven probe paused for sufficient time to allow the impact pressure to be sensed by a Statham model PM5TC $\pm$ 0.15 differential pressure transducer. Two signals, one from the Statham pressure transducer and the other a logic signal indicating that the probe was

stationary during a pause at a measuring point were recorded in analog form on magnetic tape during a run. A Honeywell model 5600C frequency modulated tape recorder was used to record and later reproduce the two signals. When reproduced, the signals were digitized using an Analogic Model AN5800 A/D converter interfaced to a Data General NOVA 840 minicomputer with 32K words of memory.

A FORTRAN program was written which sensed the digitized logic signal indicating that a measurement pause had occurred. The digitized signal representing the impact pressure was then averaged and used to compute the ratio of velocity at the impact pressure probe tip to the free stream velocity using Bernoulli's law.

C. INSTRUMENTATION FOR MEASUREMENTS OF THE WALL PRESSURE FLUCTUATIONS

Previous experience with piezoelectric pressure transducers mounted flush with the cylinder surface, Willmarth et al. (1976), indicated that piezoelectric pressure transducers are also excellent accelerometers. Elaborate precautions were necessary to prevent spurious response to mechanical vibrations of the cylinder. For this reason measurements of the wall pressure fluctuations were made with condensor microphones which are much less sensitive to vibration. The smallest available commercial microphones, Bruell and Kjaer Model 4138, have a 3.18 mm diameter diaphragm. In order to reduce the size of the sensing area a small pinhole in the cylinder surface was used to admit the wall pressure to a small cavity above the microphone diaphragm. The

microphone and preamplifier were installed within the one inch diameter cylinder as shown in Fig. 1. The diameter of the pinhole in the surface was 1.016 mm. The orifice of the pinhole microphone was exposed to an acoustic field within an anechoic chamber and calibrated (in stationary air) by comparing its output to that of another Bruell and Kjaer Model 4138, 3.18 mm diameter microphone placed nearby which had previously been calibrated using a Bruell and Kjaer Piston Phone Type 4220.

The result of the calibration is displayed in Fig. 2. There is a severe Helmholtz resonance at approximately 4.5 KHz. This was caused by the interaction of the trapped volume of air above the microphone diaphragm with the mass of air in the 1.016 mm diameter tube leading to the cylinder surface. With the aid of the calibration data of Fig. 2 we were able to correct the pinhole pressure spectra and mean square pressure for the Helmholtz resonance. As discussed later in the paper the reaction of the pinhole transducer to high frequency components of the wall pressure fluctuations was found to be large and non-uniform. This was apparently caused by an interaction between the pinhole, which represents a discontinuity in the surface, and the boundary layer. The errors were quite large when the pinhole was on the windward side of the yawed cylinder.

We also constructed a special electro-mechanical adapter for the 3.18 mm diameter microphone to allow it to be mounted flush with the surface of the one inch cylinder.

Figure 3 is a sketch of this microphone configuration showing the special 90° adapter with the 3.18 mm diameter Bruell and Kjaer microphone mounted flush with the surface and the microphone preamplifier inside the one-inch cylinder model. The additional parasitic capacitance of the adapter made it necessary to recalibrate the microphone and preamplifier. A comparison calibration was performed using the same method and equipment that was used for the pinhole microphone calibration described above. The frequency response was uniformly reduced (by a factor of 2.7) at all frequencies owing to the additional parasitic capacitance of the adapter.

The pressure fluctuation signals produced by these transducers were recorded in analog form on magnetic tape using a Honeywell Model 5600C Frequency Modulated Tape Recorder/Reproducer. The tape recorder response was uniform in the frequency band from zero to 10 KHz, however two Ithaco Model 4213 variable bandpass filters were used to reject harmonic components of the wall pressure signals below 50 Hz.

The tape recorded signals were reproduced at a later time and the power spectra were measured with a Hewlett-Packard Model 3580A Spectrum Analyzer. The wave analyzer was used with a constant bandwidth of approximately 30 Hz. The root-mean-square of the pressure signals was measured with a Thermosystems Model 1060 True Root-Mean-Square Voltmeter.

3. VELOCITY PROFILES MEASURED ON SLIGHTLY YAWED CYLINDERS

The computer controlled traversing gear described in Section 2B was used to position an impact pressure tube at various points throughout the boundary layer surrounding slightly yawed cylinders. The measurements were primarily of an exploratory nature and were designed to reveal gross features of the flow field. No attempt was made to maintain the axis of the impact pressure probe parallel to the flow. The velocity computed from the impact pressure tube pressure was obtained using Bernoulli's law. It was assumed that the static pressure everywhere in the yawed boundary layer flow was the same as the free stream static pressure. These assumptions are likely to be reasonably accurate far out in the boundary layer but may be considerably in error near the surface if the yaw angle is not small.

In all these measurements the flow in the boundary layer was turbulent. The notation for the measurements about yawed cylinders is shown in Fig. 4. All measurements were made at a station 5.5 m downstream of the test section entrance of the vertical tunnel. When the first measurements were made it was immediately discovered that the boundary layer thickness on the windward side of the cylinder was very much thinner than on the leeward side even at angles of yaw as a fraction of one degree. Figure 5 is a plot of the lines of constant velocity about a 3.175 mm diameter cylinder at a yaw angle of 1.06° measured at a station of the order of 10^3

diameters downstream from the origin of the boundary layer. The boundary layer thickness out to the $U/U_\infty = 0.95$ contour is of the order of one diameter on the windward side of the cylinder and four diameters on the leeward side. The measured boundary layer thickness out to the $U/U_\infty = 0.95$ contour at the same station at zero angle of yaw was 3 cylinder diameters, Willmarth et al. (1976). This illustrates the sensitivity of the boundary layer developed on a long cylinder to slight asymmetry of the flow.

At larger angles of yaw only the leeward boundary layer profiles were investigated. The boundary layer thickness on the windward side of the cylinder was comparable to the diameter of the impact pressure probe. Figure 6 shows the lines of constant velocity about a cylinder of 25.4 mm diameter yawed 2.36°. Although the yaw angle is very small, at $\phi = 0$ the boundary layer already has the appearance of a wake-like flow. One can observe that regions of intense velocity gradients are beginning to develop on either side of the cylinder near $\phi = 90$ and 270°.

At a yaw angle of $\alpha = 6.62°$, see Fig. 7, the development of the shear layers at $\phi = 90$ and 270° is apparently complete. In this case the estimated shear layer thickness is of the order of the diameter of the impact pressure probe. The boundary layer thickness on the windward side of the cylinder, $\phi = 180°$, must be of the order of or less than the impact probe diameter. The boundary layer thickness on the leeward (wakelike) side of the cylinder, $\phi = 0°$, is of an extent

lower than that of the uniform flow in the tunnel cross-section. In all these measurements we were able to measure only velocity contours for $U/U_\infty \leq 0.95$ with reasonable accuracy and confidence.

The flow field about the yawed 3.16 mm and 25.4 mm cylinders was surveyed for 10 other combinations of free stream velocity and yaw angle. The general features of these flows were similar to the observations shown in Figs. 5 to 7. We measured the maximum width, B, of the constant velocity contours $U/U_\infty = .95$ for each case. Figure 8 is a plot of the ratio of the wake width, B, to cylinder diameter, d, versus Reynolds number based upon cylinder diameter and free stream velocity normal to the cylinder axis, Re_n.

The ratios B/d for the 3.175 mm and 25.4 mm diameter cylinders do not lie on the same curve but do show similar behavior as a function of Re_n. Sears (1948) has shown that the laminar boundary layer equations and boundary conditions are the same for a given infinite, yawed cylinder as in a plane flow, at the same Re_n, about the cylinder at zero yaw. The plane flow solutions for the flow about any cylinder can be carried over directly to the yawed case, and the spanwise flow can be calculated by integration of linear equations. Thus, if the flow were laminar and the cylinders of infinite extent the data of Fig. 8 would all lie on the same curve. In the present investigation the flow is turbulent and Sears (1948) simplification is not possible because the (unknown) Reynolds stress terms are present in the equations for the

mean motion in the boundary layer. One would expect, intuitively, that the Reynolds stress tensor, produced by the three-dimensional turbulence in the flow, would depend upon the yaw angle, α, and azimuth angle, ϕ. Thus, the flow in the yawed cylinder boundary layer and wake cannot be as simple as it is for the laminar case discussed by Sears (1948).

The results depicted in Fig. 8 show that at small Reynolds number normal to the cylinder, Re_n, the overall width of the turbulent flow region about the cylinder is a rapidly varying function of Re_n. If Re denotes the Reynolds number based upon free stream velocity and cylinder diameter

$$Re_n = Re \sin \alpha \qquad (1)$$

Re is usually rather large, for example for a 7 cm diameter cylinder in air flowing at 30 M/sec or in water flowing at 3 M/sec, Re is of the order of 10^5. If α is small compared to 1,

$$Re_n \simeq \alpha \, Re \qquad (2)$$

In this case a yaw angle of the order of one degree will produce a Reynolds number normal to the cylinder of the order of 2×10^3. Referring to Fig. 8 the ratio B/d at one degree yaw ($Re_n \simeq 2 \times 10^3$) is very much smaller than at zero yaw angle. This illustrates the extreme sensitivity of the axially symmetric boundary layer on a cylinder to slight transverse disturbances which might be caused by free stream turbulence or by small variations in the alignment of the axis of the cylinder. The data of Fig. 8 suggest that large

changes in the character of the fluctuating flow field about cylinders may occur when the boundary layer on the cylinder is disturbed and blown or swept off the cylinder.

4. WALL PRESSURE FLUCTUATIONS ON SLIGHTLY YAWED CYLINDERS

Measurements of the wall pressure fluctuations on cylinders when the ratio δ/d is not small have been reported at zero angle of yaw by Willmarth and Yang (1970) for a three inch diameter cylinder and by Willmarth et al. (1976) for a one inch diameter cylinder. The measurements were repeated in the present investigation using the relatively large diameter flush transducer described in Section 2C mounted on a one inch diameter cylinder. In all the measurements the pressure transducer was mounted at a station 5.5 m downstream of the entrance of the test section of the vertical tunnel. We had planned to make these measurements with the much smaller diameter pinhole transducer also described in Section 2C. However, it was discovered that a severe unsteady aerodynamic interaction between the flow and the pinhole was present which caused the pressure fluctuations to attain unusually large amplitudes at high frequencies. This interaction was particularly serious when the pinhole, see Fig. 1, was on the windward side of the cylinder.

The elevated spectral levels at high frequency produced by a pinhole microphone beneath the boundary layer on a flat plate have been studied by Bull and Thomas (1976). Their paper contains information based upon a comparison between careful measurements made with a flush and a pinhole microphone of the

same diameter, d_T. Their results show that above dimensionless frequencies, $\omega\nu/u_\tau^2$, greater than 0.1 serious errors in the wall pressure spectra measured by pinhole microphones were produced. It should be noted that the nondimensional diameter of their flush and pinhole microphones, $d_T u_\tau/\nu \simeq 50$, were nearly the same as the dimensionless pinhole transducer diameter, $d_T u_\tau/\nu \simeq 60$, used in the present investigation.

All the wall pressure measurements reported in the present investigation were made with a flush transducer whose diemsnionless diameter was $d_T u_\tau/\nu = 290$. It was necessary that a flush transducer be used in this investigation especially on the windward side of the yawed cylinders. Unfortunately, we do not have flush pressure transducers as small as the pinhole diameter that are also insensitive to acceleration. It was not possible to construct a vibration isolated mounting for a very small transducer for use in the yawed cylinder measurements without great difficulty and considrable expenditure of time. We decided to use the flush condensor microphone described in Section 2C. The larger diameter of this microphone results in some loss of response at high frequencies but the ability to easily study the pressure fluctuations at any yaw or azimuth angle far outweighs the loss of high frequency response.

For reference the wall pressure spectra measured on one and three-inch diameter cylinders at zero yaw are shown in Fig. 9. There is not a large difference between the measurements at high frequency on the one-inch diameter cylinder

with the small and large flush transducers. This difference would have been larger for smaller values of $d_T u_\tau/\nu$.

Figure 10 shows the results of the root-mean-square wall pressure measured on the one-inch diameter cylinder when the yaw angle was 2.36 degrees. The root-mean-square wall pressure fluctuations were a minimum on the leeward side of the cylinder and a maximum on the windward side. The results of measurements at zero yaw are also shown in Fig. 10. The ratio of the maximum to minimum root-mean-square wall pressure was approximately 1.75. However, the root-mean-square wall pressure fluctuations on the windward side of the yawed cylinder was only a factor of 1.15 higher than on a cylinder at zero yaw. Thus, it appears that the effect of yaw on the wall pressures is a relatively large reduction in intensity on the leeward side of the yawed cylinder and a slight increase on the windward side.

The power spectrum, Eq. (5), of the "energy" in the pressure fluctuations on the yawed cylinder was also studied. Figures 11 and 12 display the power spectra of the wall pressure fluctuations measured on the yawed cylinder at free stream speeds of 35.4 and 50.3 m/sec. The units of spectral density in Figs. 11 and 12 are arbitrary but the same in each figure. Also, displayed on these figures is the spectral density at zero yaw angle. The spectral density on the leeward side, at $\phi = 0°$, is considerably lower at all frequencies than it is on an unyawed cylinder. Surprisingly, the spectral density at $\phi = 60°$ on the leeward surface of the yawed cylinder is nearly the same as that on the cylinder at zero yaw angle. On the windward side

of the cylinder, $\phi = 180°$, and at $\phi = 120°$ the spectral density is larger at high frequencies and lower at low frequencies than it is at $\phi = 60°$ or on an unyawed cylinder.

It is also noteworthy that the power spectra of the wall pressure on the cylinder yawed at an angle of 2.36 degrees shows absolutely no evidence of periodic oscillations which might be associated with the periodic shedding of vorticity. For this reason no attempt was made to observe periodic oscillations with hot wire instrumentation on the leeward side of the cylinder. Investigations of the leeward flow field at larger angles of yaw were not pursued although, according to Fig. 7, the shear layers near the leeward surfaces become more intense and vortex shedding might have been observable. On the other hand, neither Hanson (1966) nor VanAtta (1968) report observations of periodic oscillations in the wake of slightly inclined cylinders for $\alpha \leq 15°$.

In order to better compare the "shape" of the spectra measured on the yawed cylinder they have been replotted in nondimensional form and are displayed in Figs. 13 and 14. The frequency has been made dimensionless using the factor $2\pi B/U_\infty$ where B is the wake "width" (the maximum width of the $u/U_\infty = 0.95$ contour, see Fig. 8) and U_∞ is the free stream velocity. The ordinate has been multipled by $U_\infty/(B\,\overline{p^2})$. With this scaling the area under each spectrum is unity. The result of this scaling is that the "shape" of the spectra are almost the same for the case of no yaw and for the leeward

spectra, at $\phi = 0°$ and $\phi = \pm 60°$, on the yawed cylinder. On the windward surface of the yawed cylinder, at $\phi = \pm 120°$ and $\phi = 180°$, the basic shape is the same but markedly different from the leeward spectra. The amplitude is reduced at lower frequencies and increased at higher frequencies. However, at the lowest frequency the spectral amplitude appears to rapidly increase somewhat above the low frequency spectral density on the leeward surface. This increase may be caused by large scale motions of the boundary layer on the yawed cylinder which are occasionally swept off and then reappaear. We have not had time to investigate this behavior in greater detail.

There are two other important characteristics of the results displayed, Figs. 13 and 14. The first is that all the spectra scale very well with U_∞. The second is that the parameter, B, is apparently a satisfactory scaling parameter for the wall pressure on an unyawed cylinder and for the wall pressure on the leeward surface of a yawed cylinder. In these two cases the spectral shapes are the same which suggests that the character of the wall pressure fluctuations on the leeward surfaces, at small yaw angles, does not differ from the unyawed case because the boundary layer which produces these fluctuations has undergone nearly the same history during its development in passing from the windward to leeward surface as the history for the unyawed boundary layer flow development. On the other hand the boundary layer on the windward surfaces is much thinner and contains fluid which was only recently in the free stream. Therefore, the windward

surface pressure fluctuations contain more high frequency components and have in general, less energy at low frequencies.

5. WALL PRESSURE FLUCTUATIONS PRODUCED BY ISOLATED ROUGHNESS ELEMENTS

In addition to the effect of a slight flow misalignment on the wall pressure fluctuations we have also studied the effect of isolated roughness elements on the pressure fluctuations beneath the boundary layer developed on an unyawed 25.4 mm diameter cylinder. The roughness element chosen was a simple collar completely encircling the cylinder. The collars caused a step increase followed by a step decrease in cylinder diameter. Three collars were used each 50.8 mm long with thicknesses, H, of 6.35, 3.175 and 1.588 mm. In Fig. 3 a sketch of the thickest colalr, H = 6.35 mm, is shown. The collars were split in half along their length and were clamped on the cylinder by a circular metal band made from spring steel, see Fig. 3. The collars could easily be positioned at various distances, x, upstream of the stationary flush transducer, also shown in Fig. 3.

Measurements of the wall pressure fluctuations were made on the surface of the 25.4 mm diameter cylinder with the flush pressure transducer 5.5 m downstream of the exit of the contraction section of the vertical tunnel. The first measurements performed are displayed in Fig. 15 which shows the ratio of the root-mean-square pressure on the cylinder with collar installed, $\sqrt{\overline{p}_c^2}$, to dynamic pressure q_∞ as a function of dimensionless separation x/H between the downstream edge of the collar and the pressure transducer. The measurements were made at a free stream velocity of 35.36 m/sec. For this

data the ratio $\sqrt{\overline{p_c^2}}/q_\infty$ is greater than with no collar which is shown on the figure as a dashed line. The data for the different collars appear to scale very well with the collar thickness, H, and distance downstream, x.

Figure 16 shows the same data but with the pressure fluctuations produced without the collar removed. Our reasoning was that to first order the pressure fluctuations at the wall produced by the collar might simply be regarded as an uncorrelated sum or superposition of disturbances caused by the collar alone and by the cylinder without the collar. If there were no correlation between the disturbances caused by the collar alone, p_{ca}, and the pressure with no collar (i.e. $\overline{p_{ca}p_{nc}} = 0$) then the pressure fluctuations on the cylinder with the collar installed, p_c, would be;

$$p_c^2 = (\overline{p_{ca} + p_{nc}})^2 = \bar{p}_{ca}^2 + \bar{p}_{nc}^2 \quad . \tag{3}$$

The mean-square pressure fluctuations caused by the collar alone become,

$$\bar{p}_{ca}^2 = \bar{p}_c^2 - \bar{p}_{nc}^2 \quad . \tag{4}$$

Apparently, this assumption is reasonably accurate since the data measured with different collars appear to be self consistent, see Fig. 16. Figures 15 and 16 show that a considerable increase in the fluctuating wall pressure is produced by isolated roughness elements which are less than one quarter of the cylinder diameter in thickness.

The next phase of these measurements was a systematic study of the power spectra of the disturbances produced by the three collars. The power spectrum, $F(\omega)$, is the Fourier transform of the auto correlation of the wall pressure fluctuations,

$$F(\omega) = \frac{2}{\pi} \int_0^\infty \overline{p(t)p(t + \tau)} \cos \omega\tau \, d\tau \qquad (5)$$

and it is assumed that $p(t)$ is a stationary random function. The inverse transform is

$$\overline{p(t)p(t + \tau)} = \int_0^\infty F(\omega) \cos \omega\tau \, d\omega \qquad (6)$$

Figures 17, 18, and 19 display the power spectra of the wall pressure measured on the cylinder surface with the three collars installed at various distances upstream of the pressure transducer. The units of the power spectra (the ordinates) are arbitrary but are the same in each of the three figures to allow a comparison between them. The data are of relatively high quality, since a linear scale can be used for the ordinate. The spectral density at low frequencies, less than 1000 Hz, is relatively large and shows a rapid increase as the frequency is reduced. The spectral density measured on the cylinder without a collar is also shown for reference on each plot. The magnitude of the low frequency disturbance produced by the collar is considerable. For example, the spectral density measured at $x/H = 9$ for the collar with $H/d = 0.25$ is a maximum of 10.5 times the spectral density without the collar at a low frequency of the order of 1 KHz.

The relatively high quality and consistency of the data of Figs. 17, 18, and 19, suggests that an approximate scaling of the power spectra with free stream velocity, collar height and distance downstream of the collar may be valid. We made a number of different plots of the data and found that in addition to the above scaling it was also possible to subtract the power spectrum measured without the collar from that measured with the collar and still maintain a reasonably consistent scaling. In order to understand the subtraction of the power spectra one may use a result analogous to Eq. (3) which is based on the assumption that the correlation between the wall pressure fluctuations produced by the collar alone and without a collar is zero, $\overline{p_{ca}(t_1)p_{nc}(t_2)} = 0$, for any time delay. It can then be shown that the power spectrum caused by the collar alone, $F_{ca}(\omega)$, is simply

$$F_{ca}(\omega) = F_{c}(\omega) - F_{nc}(\omega) \qquad (7)$$

The power spectrum of the collar alone, $F_{ca}(\omega)$, was nondimensionalized in terms of the characteristic frequency corresponding to the ratio of free stream velocity to collar thickness, U_∞/H. It was then discovered that if the power spectra of the collar alone data, $F_{ca}(\omega)$, were normalized to unit area the shape of the resulting spectra for a given value of x/H were approximately the same. These data have been plotted in Figs. 20 through 26 for values of x/H from 8 to 240.

In Figs. 20 through 26 the ordinate is given the label C in order to save writing. In terms of the power spectral

density and scaling parameters the ordinate is,

$$C = U_\infty F_{ca}(\omega)/(H \bar{p}_{ca}^2) \tag{8}$$

and the area beneath the power spectral density curves of Figs. 20 through 26 is unity,

$$\int_0^\infty C \, d(\omega H/U_\infty) = \int_0^\infty U_\infty F_{ca}(\omega)/(H \bar{p}_{ca}^2) \, d(\omega H/U_\infty) = 1 \tag{9}$$

since

$$\int_0^\infty F_{ca}(\omega) \, d\omega = \bar{p}_{ca}^2 \tag{10}$$

The results of the normalized spectral measurements of the pressure fluctuations on the wall at a stream speed of 35.4 m/sec and at a distance, x, equal to 8 collar thicknesses downstream of the collar are shown in Fig. 20. The spectra have nearly the same shape for collar thicknesses of d/4 and d/8 but for the thinnest collar, d/16, the shape is different. This indicates that the scaling on outer variables, H and U_∞, is not valid for the thin collar at x = 8H. This collar is well within the wall region of the boundary layer since its thickness is only 160 viscous lengths, i.e. $Hu_\tau/\nu \simeq 160$. This suggests that for small roughness heights the disturbance produced should be scaled with wall variables ν and u_τ. Mulhearn (1976) has investigated wall pressure fluctuations downstream of an abrupt change in surface roughness. He found that an internal layer of disturbances occurred within the boundary layer which increased in magnitude as they were

carried downstream. The disturbances reached a maximum and then decreased as a new equilibrium boundary layer above the rough surface was formed. Antonia and Luxton (1971) investigated the fluctuating velocity field downstream of an abrupt change from smooth to upstanding roughness elements on the surface everywhere downstream. He found a similar internal layer of new disturbances growing within the existing boundary layer.

We did not investigate the scaling of smaller disturbances using wall variables related to internal layers in the present series of measurements. Instead, the case of larger scale disturbances, produced by thicker collars, which scale on the outer variables were studied in some detail.

Figure 21 displays the spectra for the collar alone when the wall pressure fluctuations were measured 16 collar thicknesses downstream. Again the spectrum for the thinnest collar does not agree very well with those for the thicker collars. As one proceeds further downstream, Figs. 22, 23, 24, and 25, all three of the spectra are similar to one another. Presumably the disturbances from the thin collar have now grown large enough to scale on outer variables. Another change that occurs is that for larger distances downstream of the collar more energy begins to appear at very low frequencies. The scaling for this data appears to be consistent and it is suggested that a similar scaling should be valid for other types of large isolated roughness elements. The agreement among the data is quite consistent.

The data displayed in Fig. 26 were obtained at a point 240 collar thicknesses downstream of the collar. The normalized spectra are still approximately similar to one another but their shape is appreciably different from the shape measured further upstream. This data suggests that there is a continual evolution of the harmonic content of the wall pressure fluctuations produced by isolated roughness elements. From a practical point of view the results at large distances downstream may not be too important because, as is observed in Fig. 16, the wall pressure fluctuations caused by the roughness elements have become quite small, at distances of the order of $x/H \simeq 200$.

6. CONCLUSIONS

1. Measurements of the shape of the iso-velocity contours about yawed cylinders show the development of marked asymmetry even for very small angles of yaw, see Fig. 8. This suggests that the fluctuating flow properties within the boundary layer on a long cylinder may be very dependent upon disturbances in the free stream or upon variations in yaw angle caused by the cylinder axis not being perfectly straight.

2. The intensity of the wall pressure fluctuations measured on the windward side of a cylinder yawed at an angle of 2.36 degrees were only slightly increased above the unyawed results. On the leeward side the intensity was well below the intensity measured with no yaw.

3. The harmonic content of the wall pressure spectra is large at high frequencies over most of the windward surface of a yawed cylinder and is largest at low frequencies on the leeward position at $\phi = 0$. At an intermediate position 60 degrees from the leeward position, i.e. $\phi = \pm 60°$, the harmonic content of the spectra are similar to the unyawed case but the overall intensity of the fluctuation is reduced.

4. A pinhole microphone was found to produce very large spurious pressure fluctuation signals when it was located on the windward surface of a yawed cylinder.

Unfortunately, the smallest suitable flush pressure transducer available for the present measurements, $d_T = 290\ \nu/U_\tau$, was not small enough to completely resolve the high frequency (small scale) harmonic components of the wall pressure fluctuations on the windward surface of the cylinder.

5. Large isolated roughness elements on an unyawed cylinder produce a large increase in the intensity of the wall pressure fluctuations well downstream. The intensity which decreases as the distance downstream is increased scales with the dimensionless downstream distance, x/H.

6. The power spectra of the pressure fluctuations caused by the larger collars scale with the characteristic frequency U_∞/H which is based on the flow speed characteristic of the outer part of the boundary layer. There is a small amount of data which suggests that for smaller isolated roughness elements the spectra may scale with the wall variables ν and u_τ. (The characteristic frequency would then be u_τ^2/ν.)

ACKNOWLEDGMENTS

We wish to acknowledge the skillful work of Mr. Casey Samborski who constructed the flow traversing mechanism and various microphone adapters and that of Mr. John Van Roekel who designed the computer software and the interface between the minicomputer and traversing mechanism. We are very grateful to the Office of Naval Research whose continuous support has made this investigation possible.

REFERENCES

Antonia, R.A. and Luxton, R.E. (1971), "The Response of a Turbulent Boundary Layer to an Upstanding Step Change in Surface Roughness," J. Basic Eng. Trans. ASME, 93, 22.

Bull, M.K. and Thomas, A.S.W., "High Fruequency Wall-Pressure Fluctuations in Turbulent Boundary Layers," Phys. of Fluids 19, 4, 597.

Hanson, A.R. (1966), "Vortex Shedding from Yawed Cylinders," J. Am. Inst. Aero Astro. 4, 4, 738.

Mulhearn, P.J. (1976), "Turbulent Boundary Layer Wall-Pressure Fluctuations Downstream from an Abrupt Change in Surface Roughness," Phys. Fluids 19, 6, 796.

Reid, R.O. and Wilson, B.W. (1963), "Boundary Layer Flow Along a Circular Cylinder," J. Hyd. Div. Proc. Am. Soc. of Civil Eng., 3, 21.

Sears, W.R. (1948), "The Boundary Layer on Yawed Cylinders," J. Aero. Sci. 15, 1, 49.

Van Atta, C.W. (1968), "Experiments on Vortex Shedding from Yawed Circular Cylinders," J. Am. Inst. Aero. Astro. 6, 5, 931.

Willmarth, W.W. and Yang, C.S. (1970), "Wall Pressure Fluctuations Beneath Turbulent Boundary Layers on a Flat Plate and a Cylinder," J. Fluid Mech. 41, 47.

Willmarth, W.W., Winkel, R.E., Sharma, L.K., and Bogar, T.J. (1976), "Axially Symmetric Turbulent Boundary Layers on Cylinders: Mean Velocity Profiles and Wall Pressure Fluctuations," J. Fluid Mech. 76, 35.

Figure 1. Sketch of 45° pinhole microphone configuration and construction: A, pinhole of diameter 1.02 mm at surface of cylinder; B, plastic cover over microphone adapted from Bruell and Kjaer pistonphone seal type DB-0352; C, Bruell and Kjaer Microphone Model 4138; D, rubber seal within part B; E, Bruell and Kjaer adapter type UA0160; F, Bruell and Kjaer preamplifier type 2618; G, stranded steel cable under tension used to hold cylinder model together; H, 25.4 mm diameter aluminum cylinder model; J, plastic fitting used to align cylinder halves.

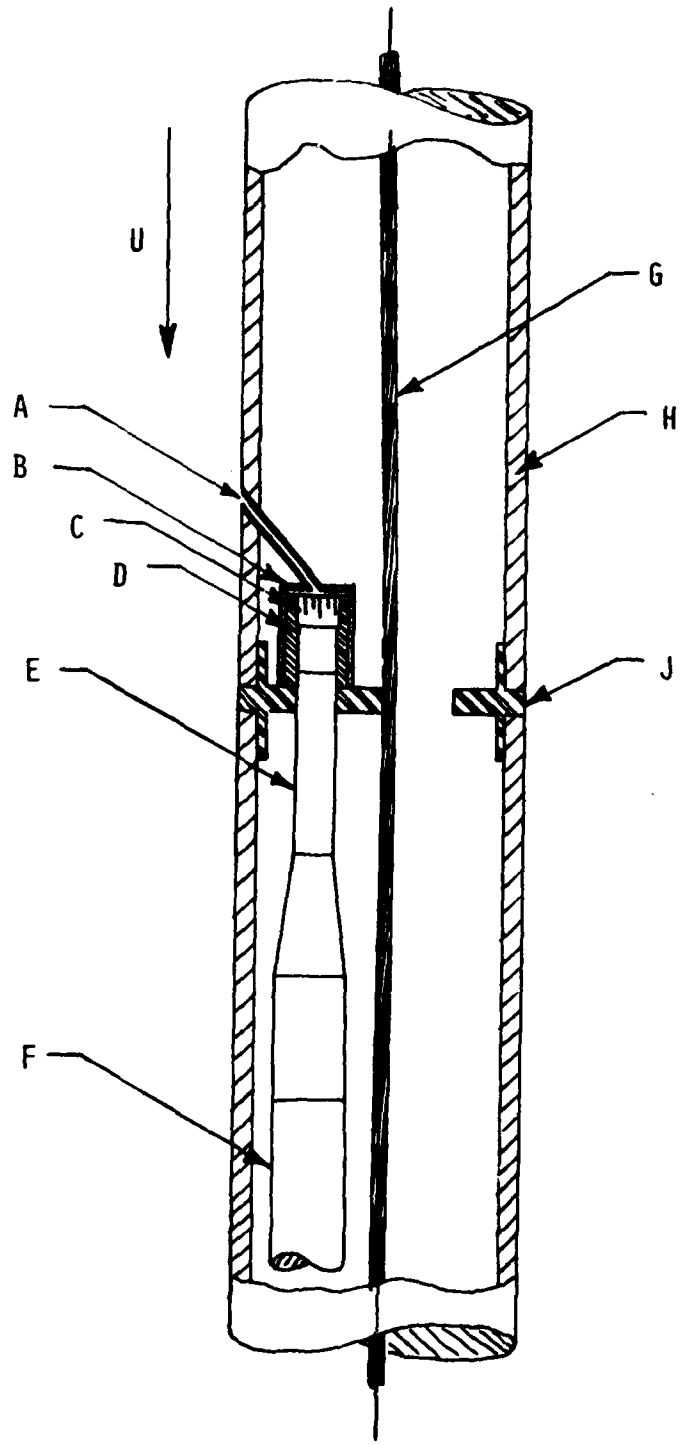

FIGURE 1

Figure 2. Frequency response calibration data for pinhole microphone. Ordinate is ratio of pinhole microphone output to flush microphone output.

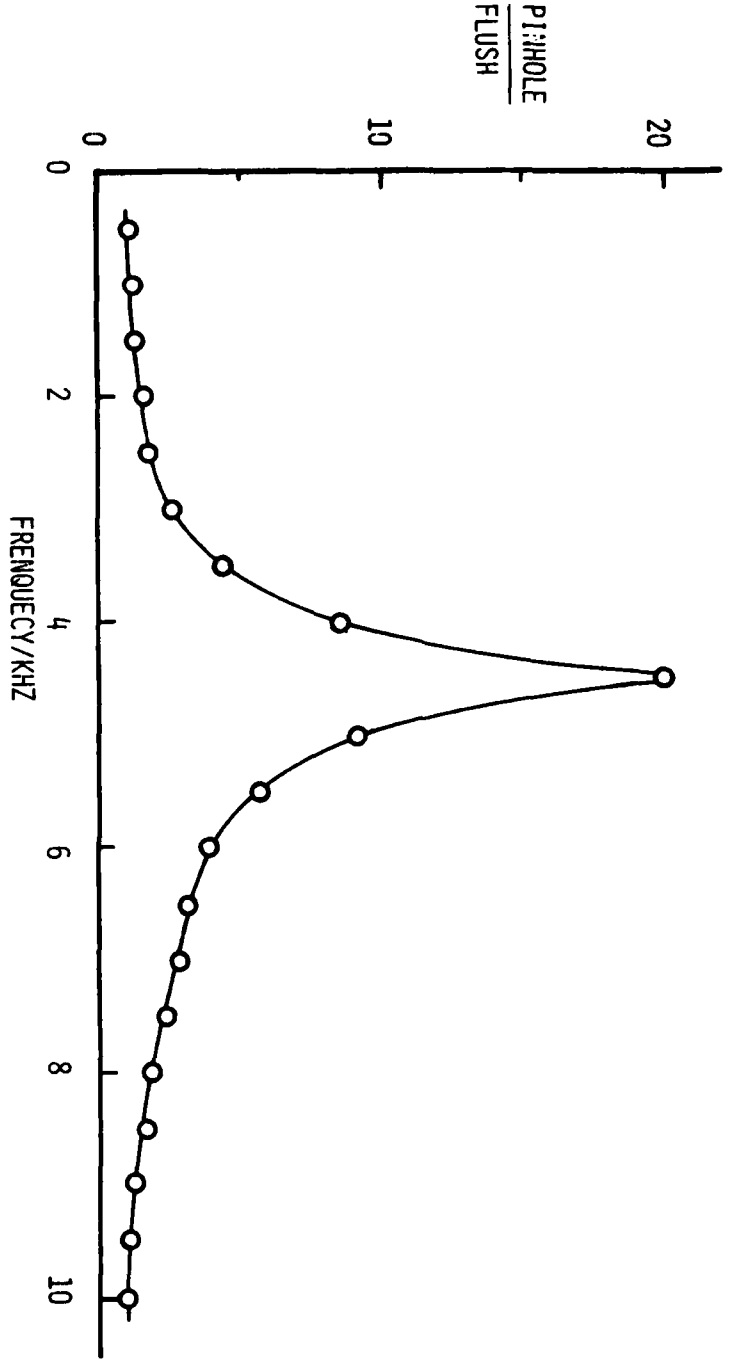

FIGURE 2

Figure 3. Sketch of flush microphone configuration and collar configuration and construction: A, aluminum collar, two halves; B, flat steel spring clamps collar halves to cylinder; C, stranded steel cable under tension holds cylinder model together; D, 25.4 mm diameter aluminum cylinder model; E, electromechanical adapter for Bruell and Kjaer microphone and preamplifier; F, attachment to hold preamplifier on part E; G, Bruell and Kjaer preamplifier type 2618; J, Bruell and Kjaer microphone model 4138, 3.175 mm diameter.

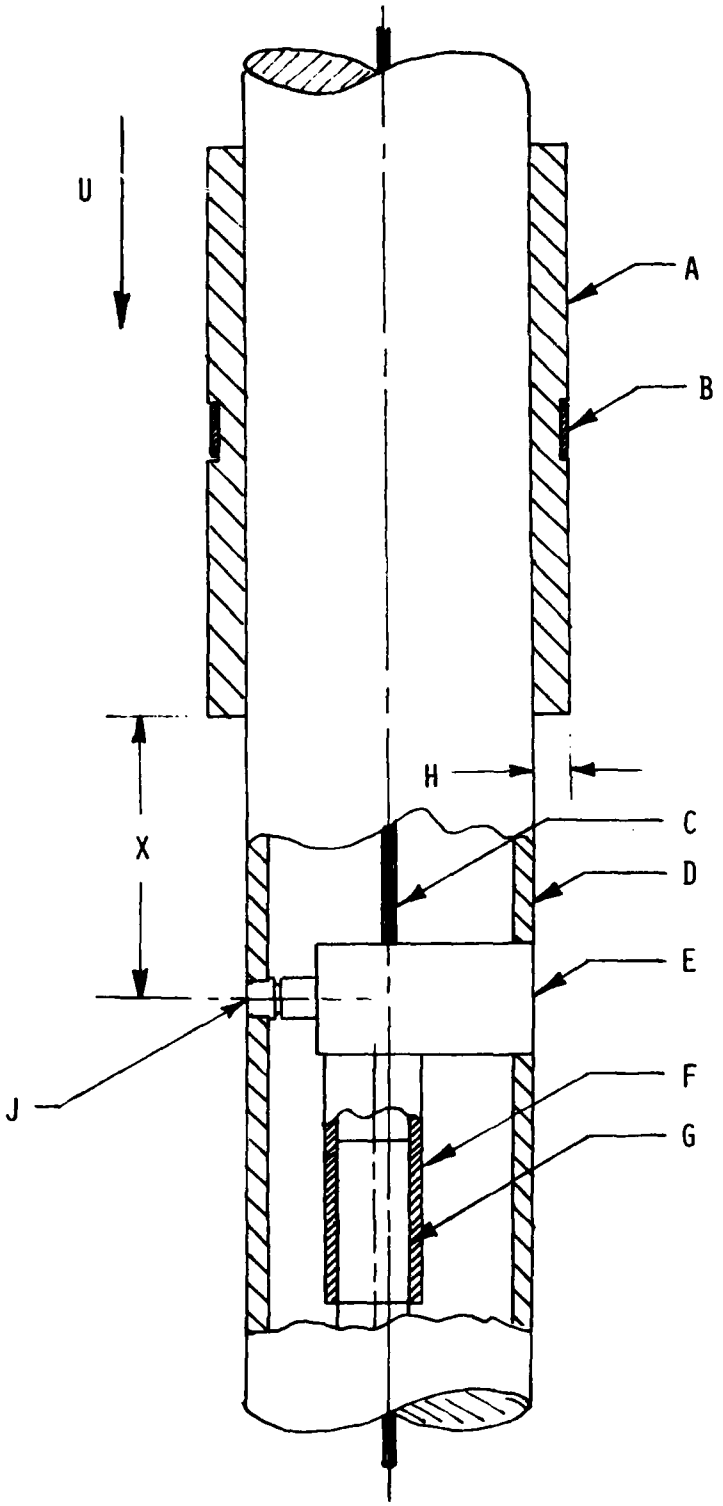

FIGURE 3

Figure 4. Sketch of yawed cylinder showing coordinate notation.

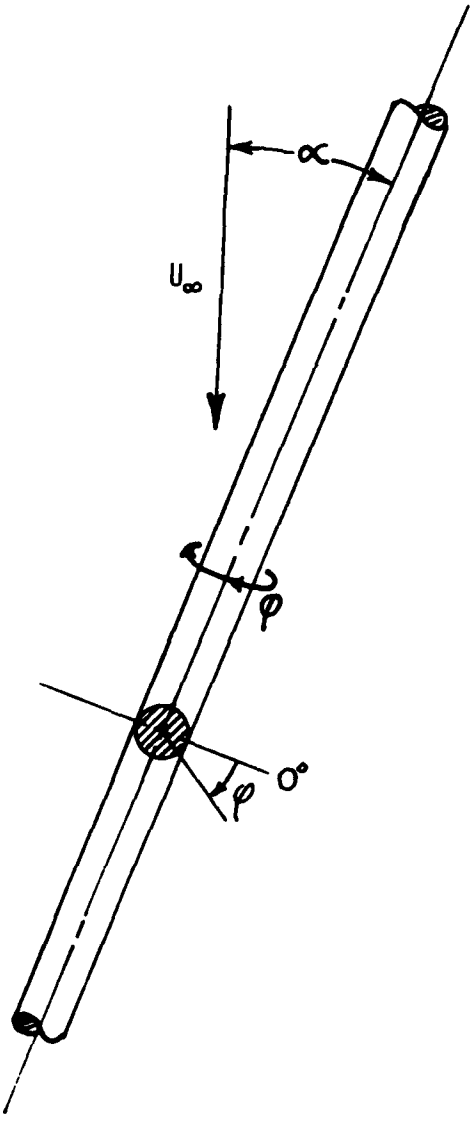

FIGURE 4

Figure 5. Lines of constant velocity about a 3.175 mm diameter cylinder. $\alpha = 1.06°$, $U_\infty = 46.88$ m/sec, $Re_n = 180.8$.

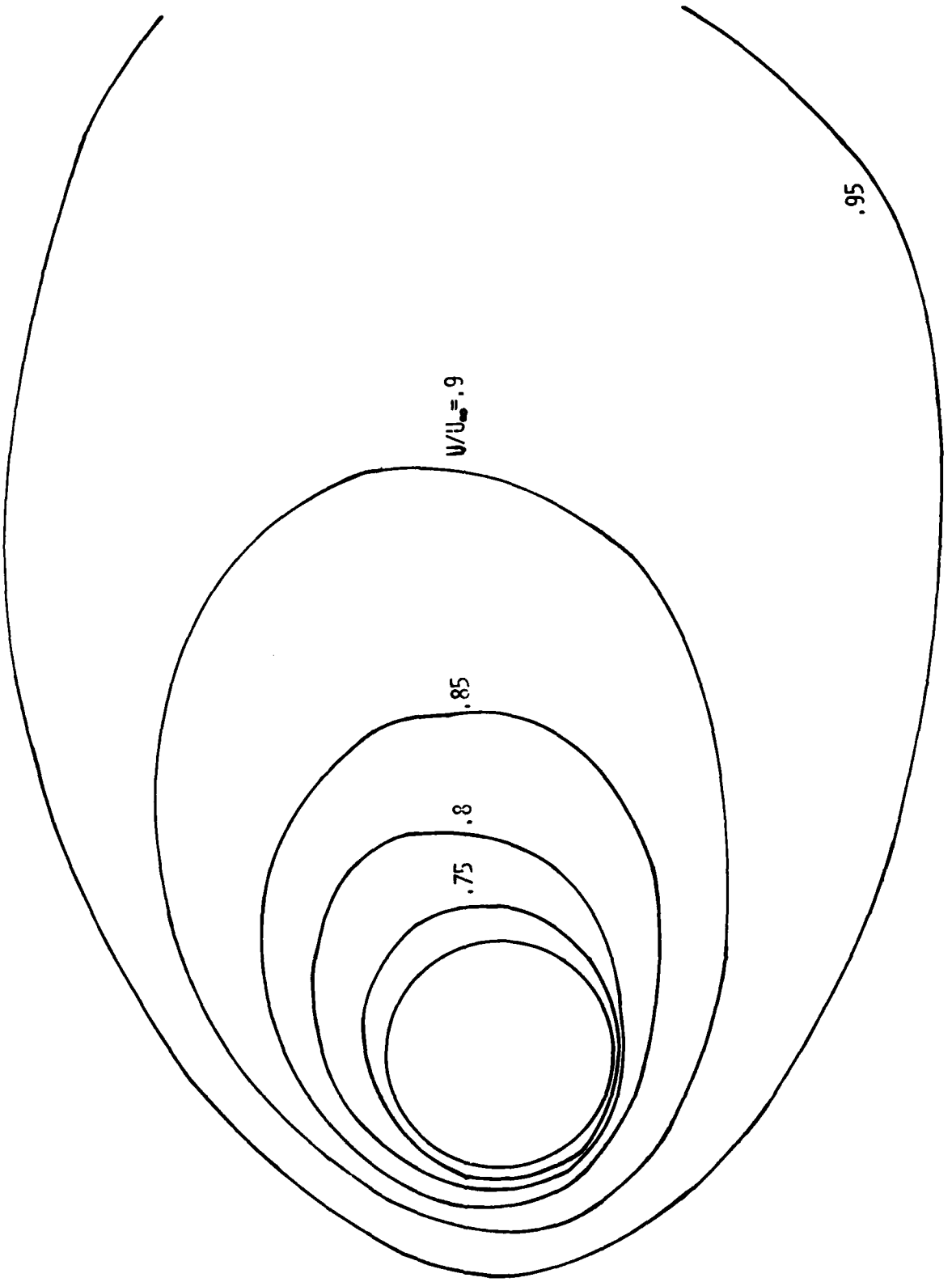

FIGURE 5

Figure 6. Lines of constant velocity about a 25.4 mm diameter cylinder. $\alpha = 2.36°$, $U_\infty = 47.85$ m/sec, $Re_n = 3240$.

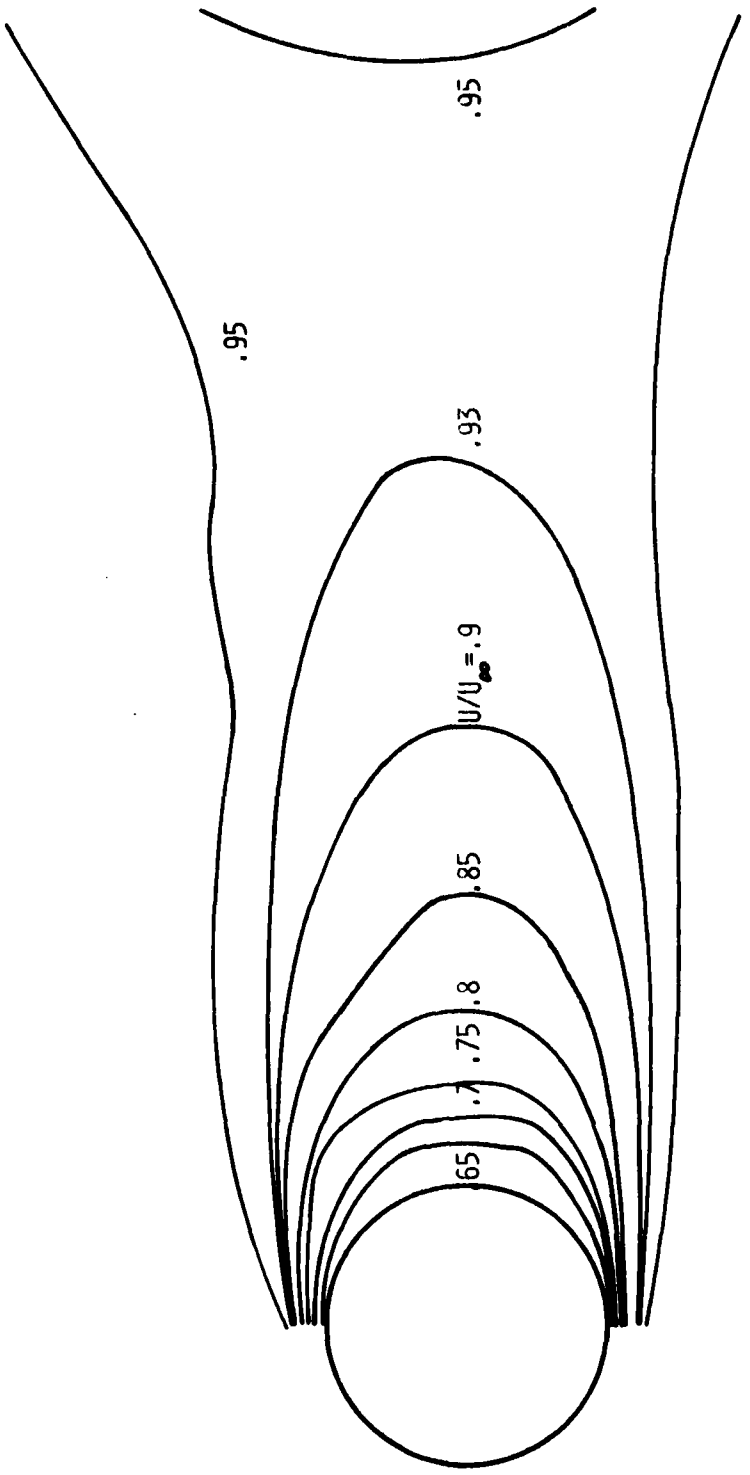

FIGURE 6

Figure 7. Lines of constant velocity about a 25.4 mm diameter cylinder. $\alpha = 6.62°$, $U_\infty = 47.85$ m/sec, $Re_n = 9048$.

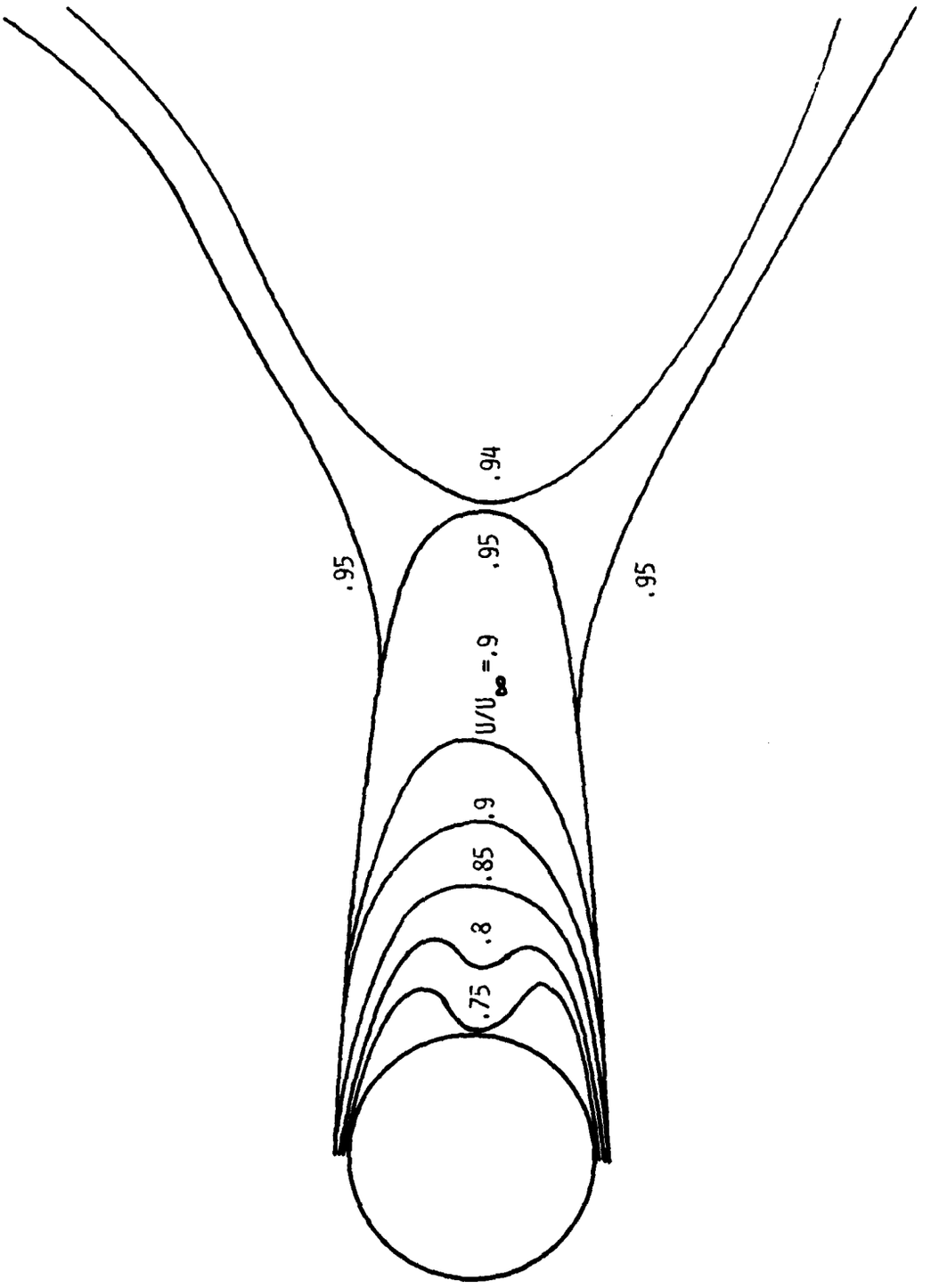

FIGURE 7

Figure 8. Ratio of retarded flow region width, B, (width of u/U_∞ = .95 contour) to cylinder diameter, d, for a cylinder length, ℓ, of 5.5 meters as a function of Reynolds number, Re_n, based upon d, and the velocity normal to the cylinder. O , d = 3.18 mm, ℓ/d = 1380; ● , d = 25.4 mm, ℓ/d = 217.

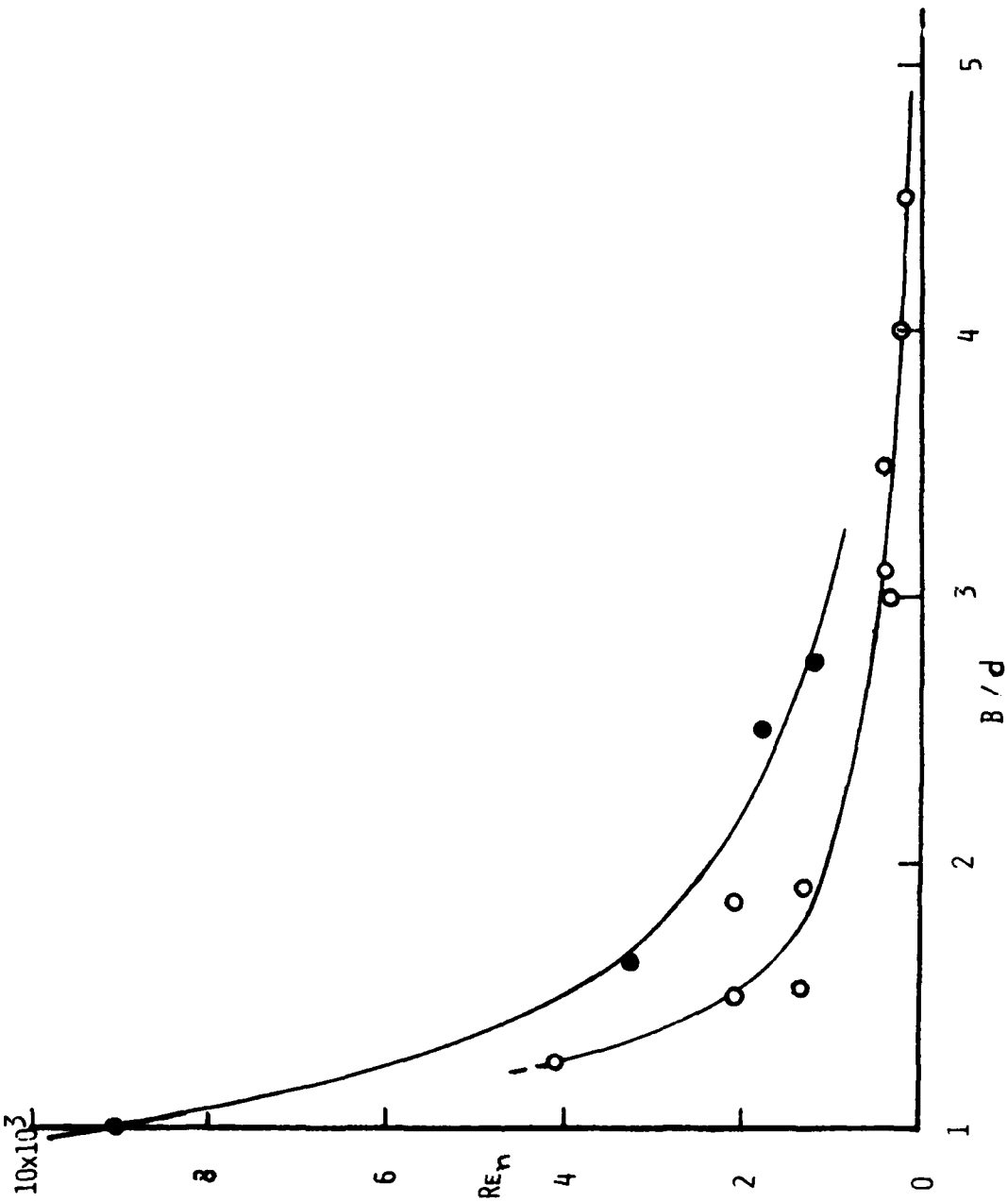

FIGURE 8

Figure 9. Dimensionless wall pressure spectra at zero angle of yaw measured with flush microphones. O , 25.4 mm diameter cylinder $d_T u_\tau/\nu$ = 190 [Willmarth et al. (1976)]; ◓ , 76.2 mm diameter cylinder $d_T u_\tau/\nu$ = 158 [Willmarth and Yang (1970)]; ● , present measurements one inch diameter cylinder $d_T u_\tau/\nu$ = 290.

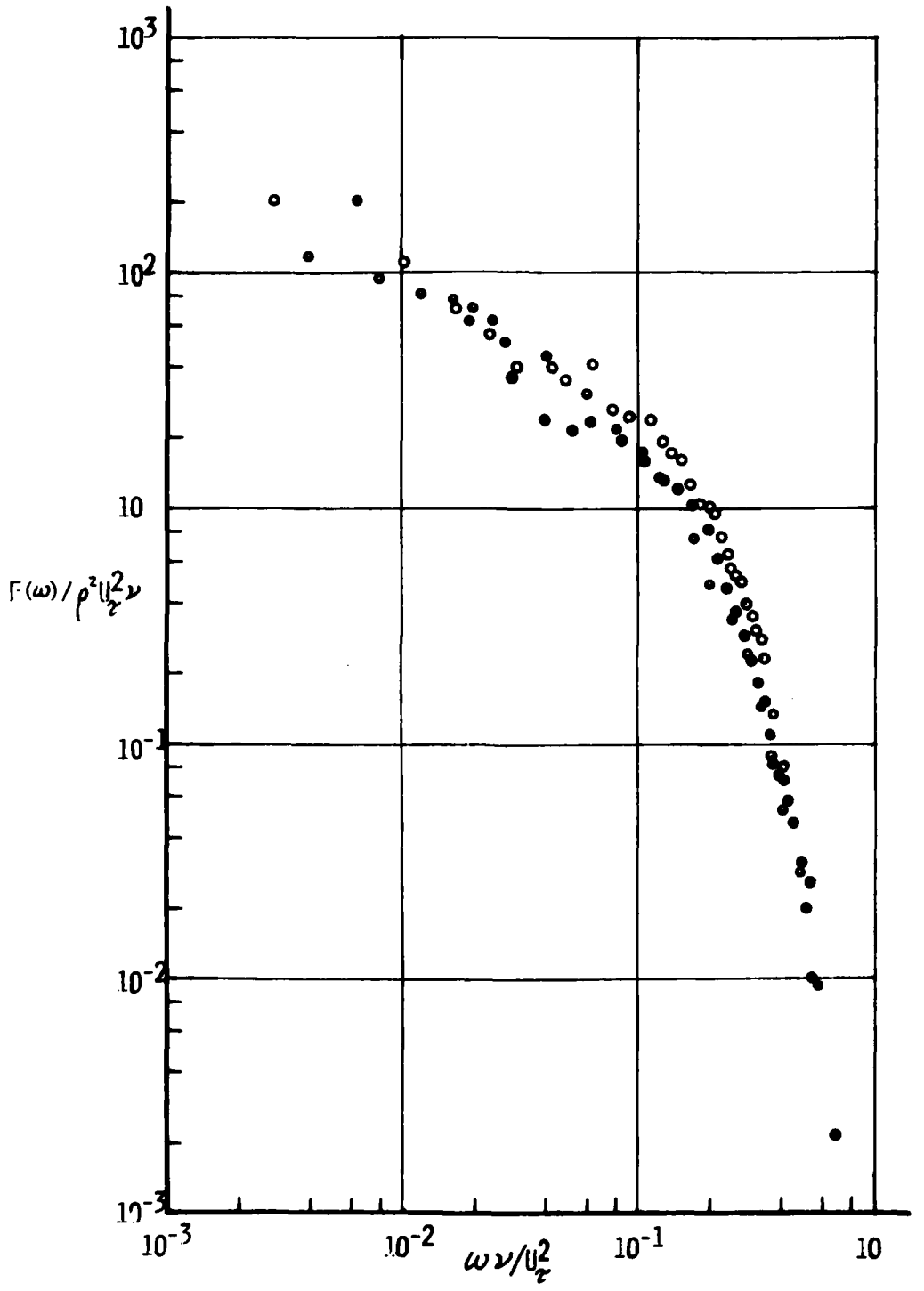
10^3
10^2
10
10^{-1}
10^{-2}
10^{-3}
$\Gamma(\omega)/\rho^2 u_\tau^2 \nu$
10^{-3}
10^{-2}
10^{-1}
10
$\omega\nu/u_\tau^2$

FIGURE 9

Figure 10. Root-mean-square wall pressure measured on a 25.4 mm diameter cylinder. Transducer is flush with surface and of diameter $d_T = 290\ \nu/u_\tau$. O , $\alpha = 2.36°$, $U_\infty = 35.36$ m/sec; ● , $\alpha = 2.36°$, $U_\infty = 50.29$ m/sec; – – – –, $\alpha = 0$, $U_\infty = 35.36$ m/sec; ———, $\alpha = 0$, $U_\infty = 50.29$ m/sec.

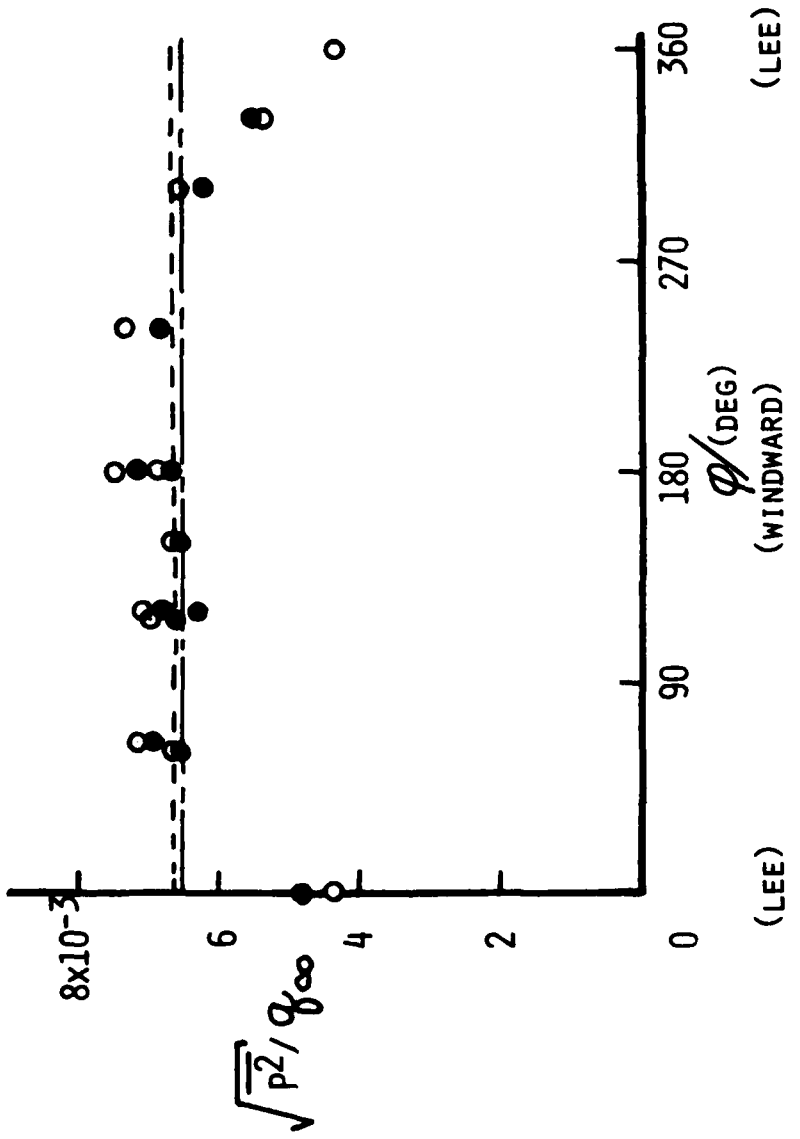
8x10⁻³
6
4
2
0
$\sqrt{\overline{p^2}}/q_\infty$
90
180
270
360
ϕ (DEG)
(LEE)
(WINDWARD)
(LEE)

FIGURE 10

Figure 11. Power spectral density on 25.4 mm diameter cylinder yawed at 2.36°. A is the amplitude of spectral density in arbitrary units at free stream velocity of 35.4 m/sec. *, ϕ = 0°; @, ϕ = 60°; #, ϕ = 120°; +, ϕ = 180°. The symbol Ø is the spectral density on an unyawed cylinder.

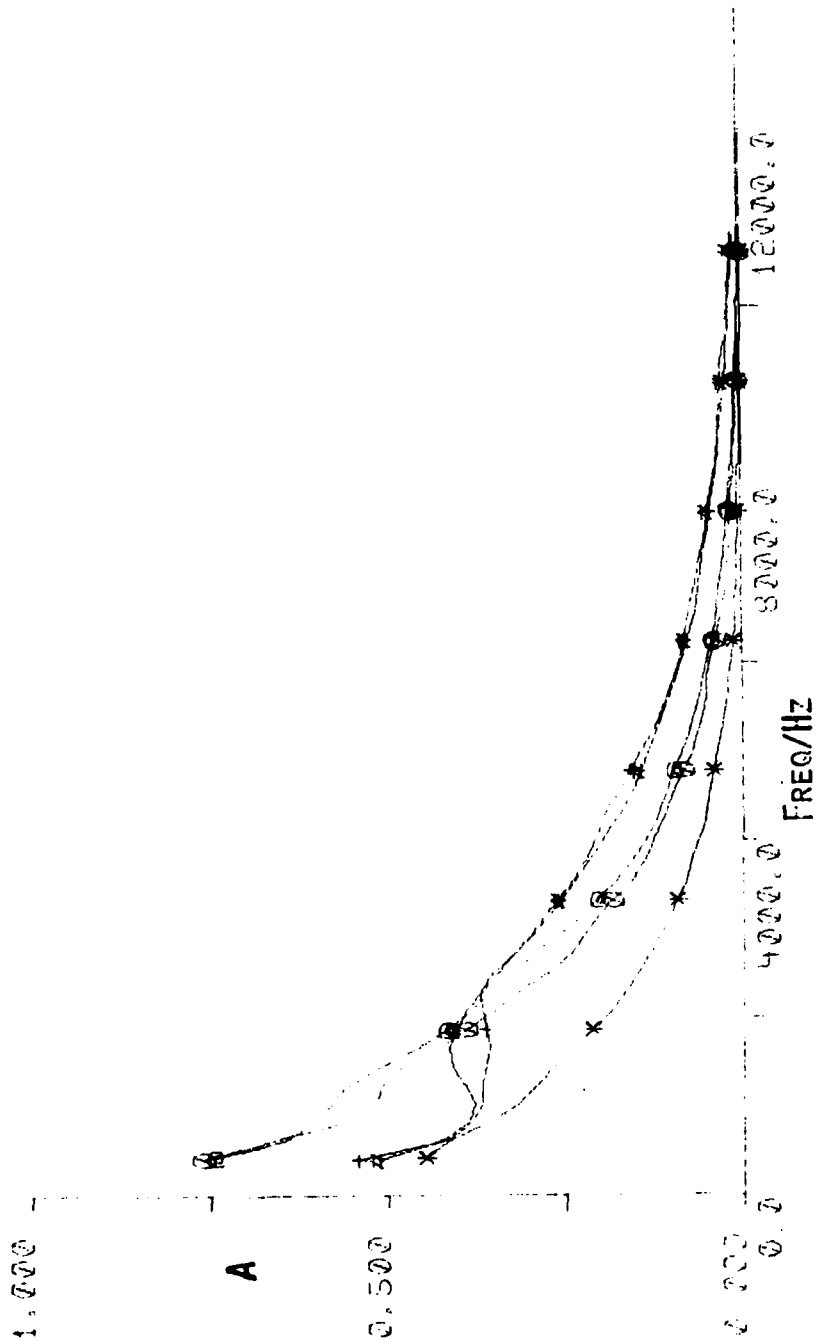

FIGURE 11

Figure 12. Caption and symbols same as Figure 11 except that the free stream velocity is 50.3 m/sec for this plot.

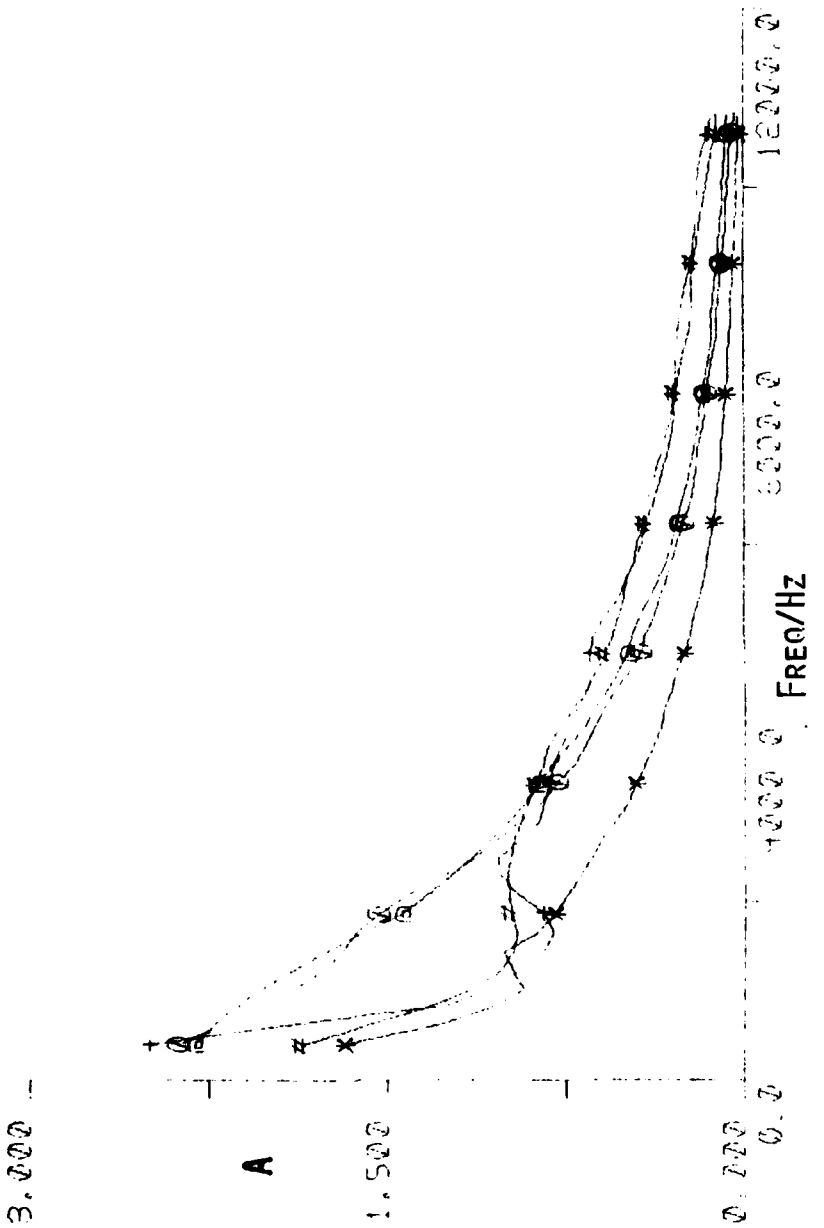

FIGURE 12

Figure 13. Nondimensional spectral density on the 25.4 mm diameter cylinder yawed at 2.36° at free-stream velocity of 35.4 m/sec. Symbols same as Figs. 11 and 12.

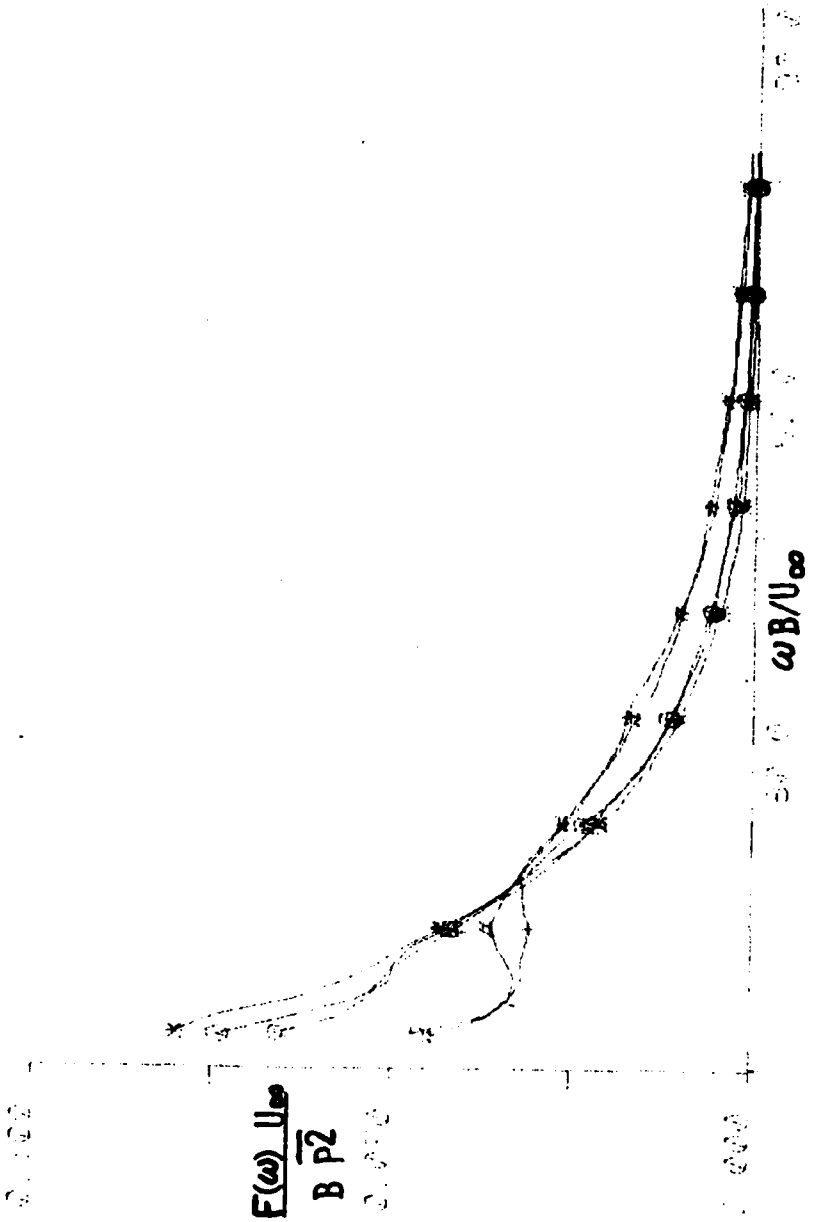

FIGURE 13

Figure 14. Caption and symbols same as Fig. 13 except that the free stream velocity is 50.3 m/sec for this plot.

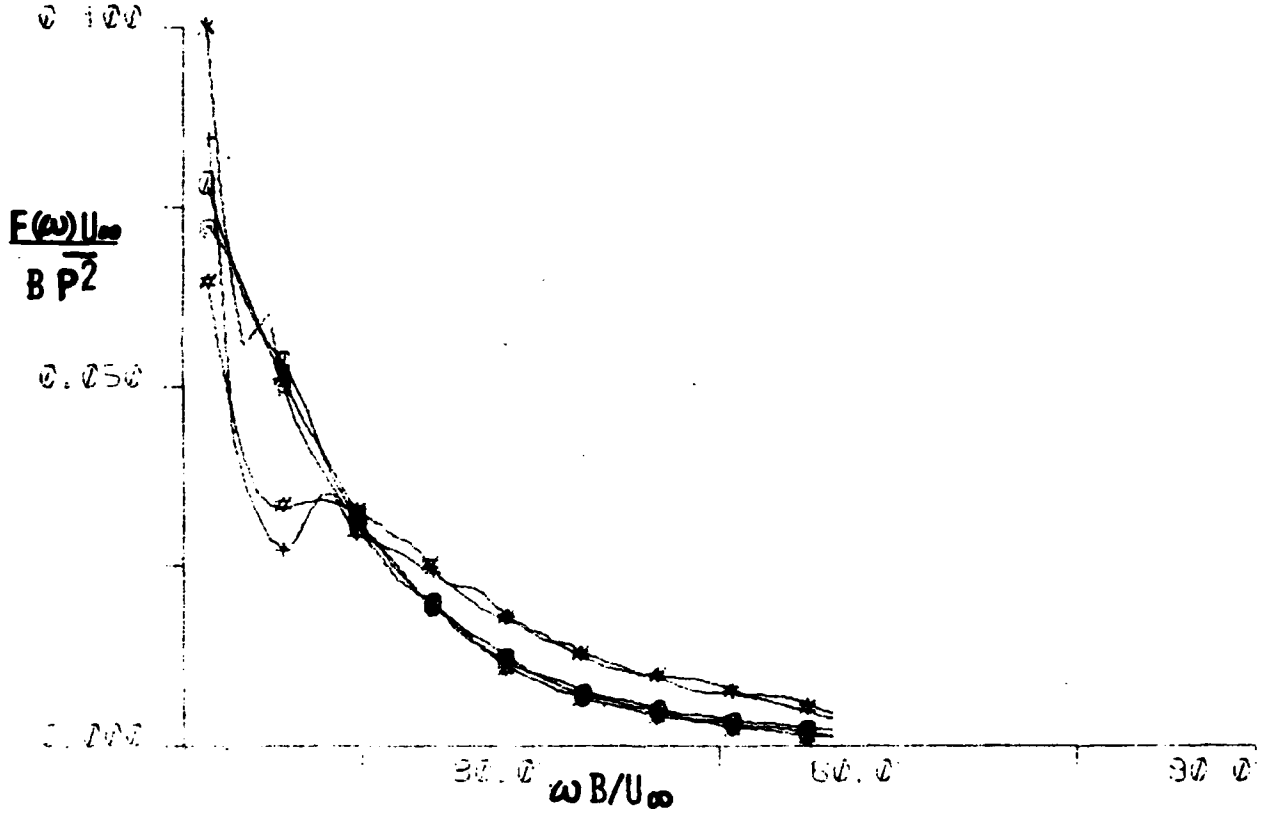

FIGURE 14.

Figure 15. Root-mean-square wall pressure fluctuations at various distance, x, downstream of isolated roughness elements with three different thicknesses, H. O , H/d = 0.25; ● , H/d = 0.125, × , H/d = 0.063,—·—, no collar.

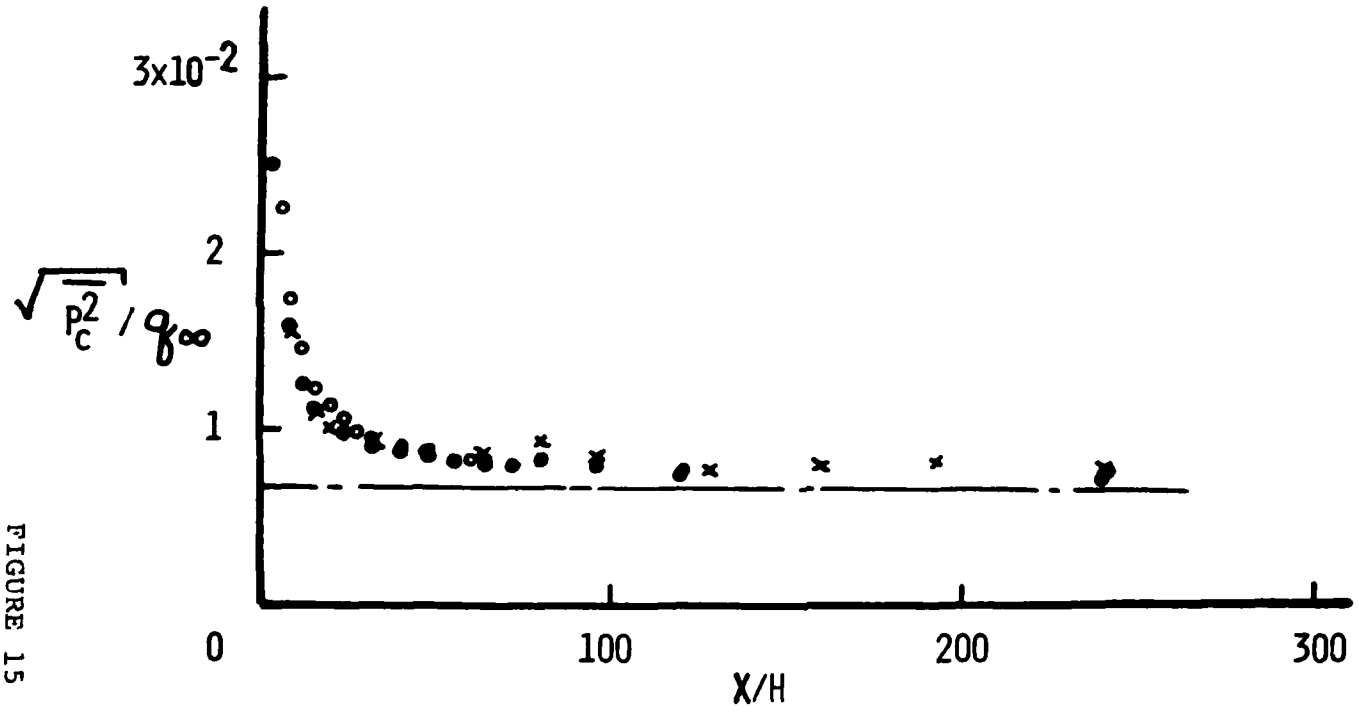

FIGURE 15

Figure 16. Root-mean-square wall pressure fluctuations at various distances, x, downstream of isolated roughness elements with three different thicknesses, H, after subtraction of the pressure fluctuations measured without the collar. O , H/d = 0.25; ● , H/d = 0.125; × , H/d = 0.063.

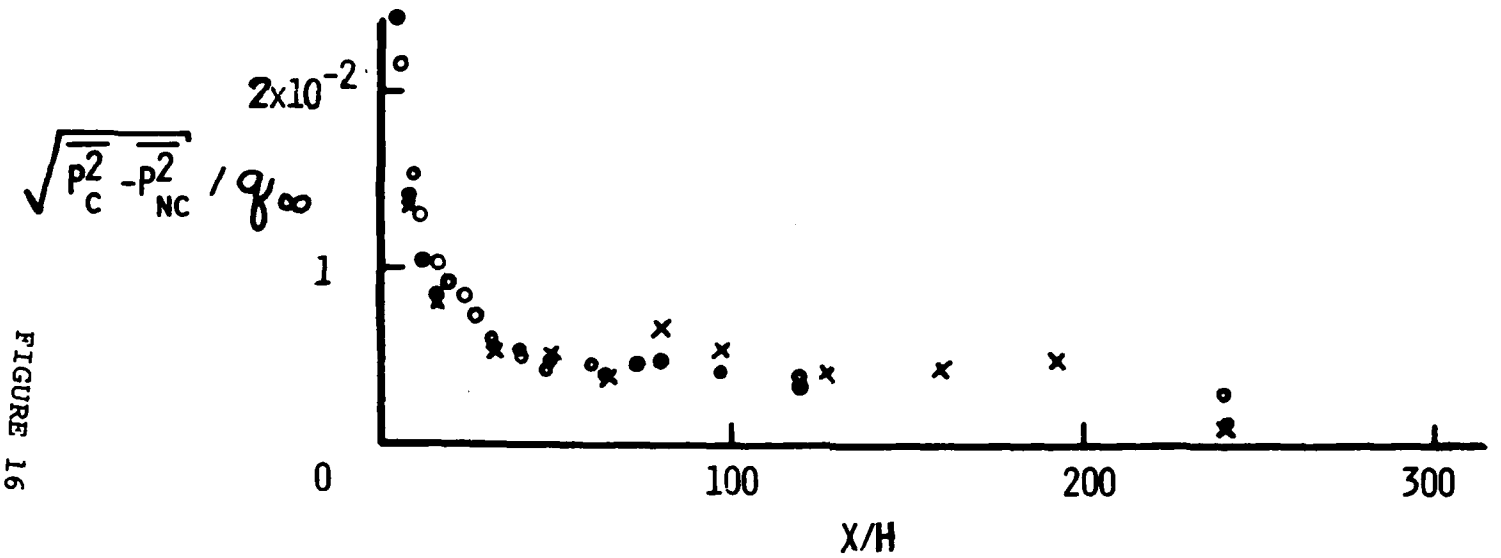
$\sqrt{\overline{P_C^2} - \overline{P_{NC}^2}} / q_\infty$
2×10^{-2}
1
0
100
200
300
X/H

FIGURE 16

Figure 17. Power spectral density of the wall pressure fluctuations at various distances downstream of a collar. Collar height, H = 0.25d = 6.35 mm. *, x/H = 9; @, x/H = 20; #, x/H = 40; +, x/H = 120; Ø, no collar. A, the magnitude of the power spectral density is arbitrary but of the same scale factor for all the data.

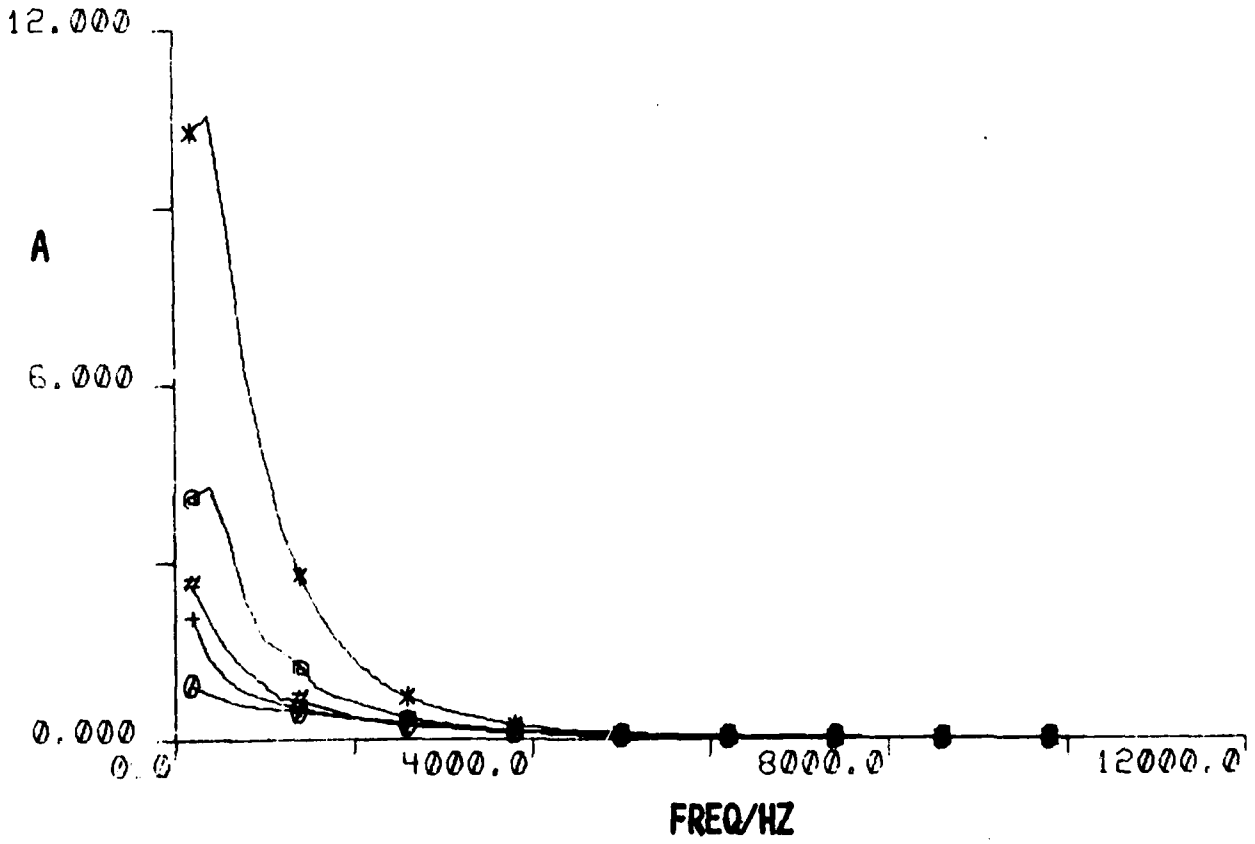

FIGURE 17

Figure 18. Caption the same as Fig. 17 except that collar height H = 0.125d = 3.175 mm. *, x/H = 16; @, x/H = 20; #, x/H = 80; +, x/H = 240; Ø, no collar.

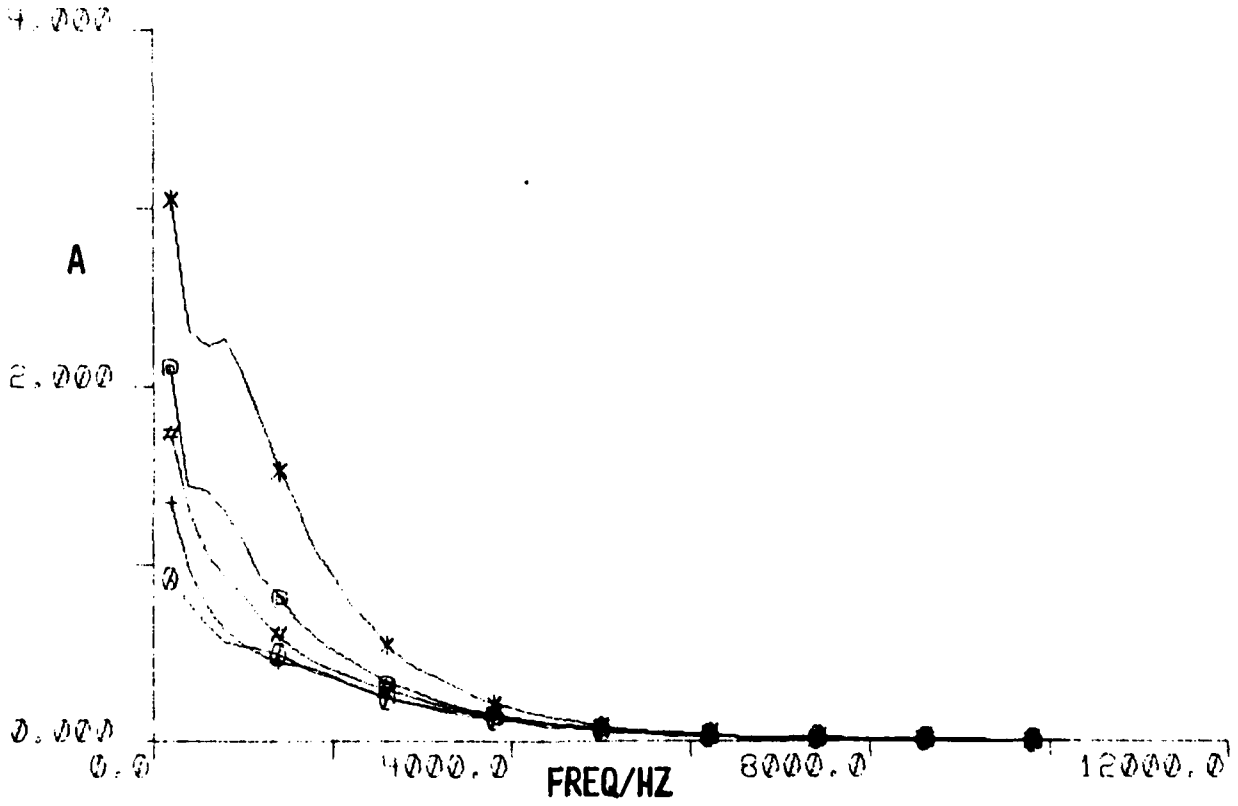

FIGURE 18

Figure 19. Caption the same as Fig. 17 except that the collar height H = 0.063d = 1.588 mm. *, x/H = 32; @, x/H = 80; Ø , no collar.

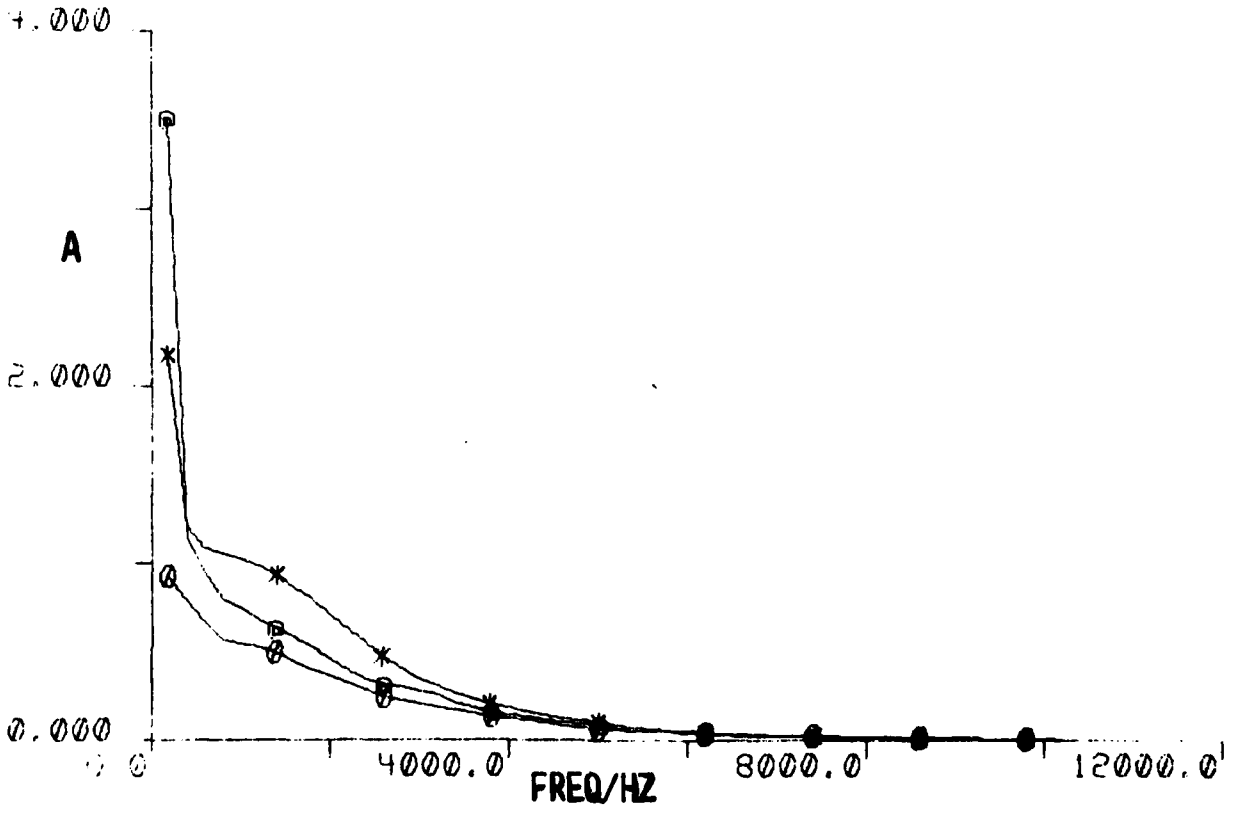

FIGURE 19

Figure 20. Normalized nondimensional power spectra of the additional wall pressure fluctuations produced by the collars of various thicknesses. Distance downstream of collar is x/H = 8. +, H/d = 0.25; *, H/d = 0.125; Ø , H/d = 0.063. The ordinate C is $U_\infty F(\omega)/H\overline{p^2}$.

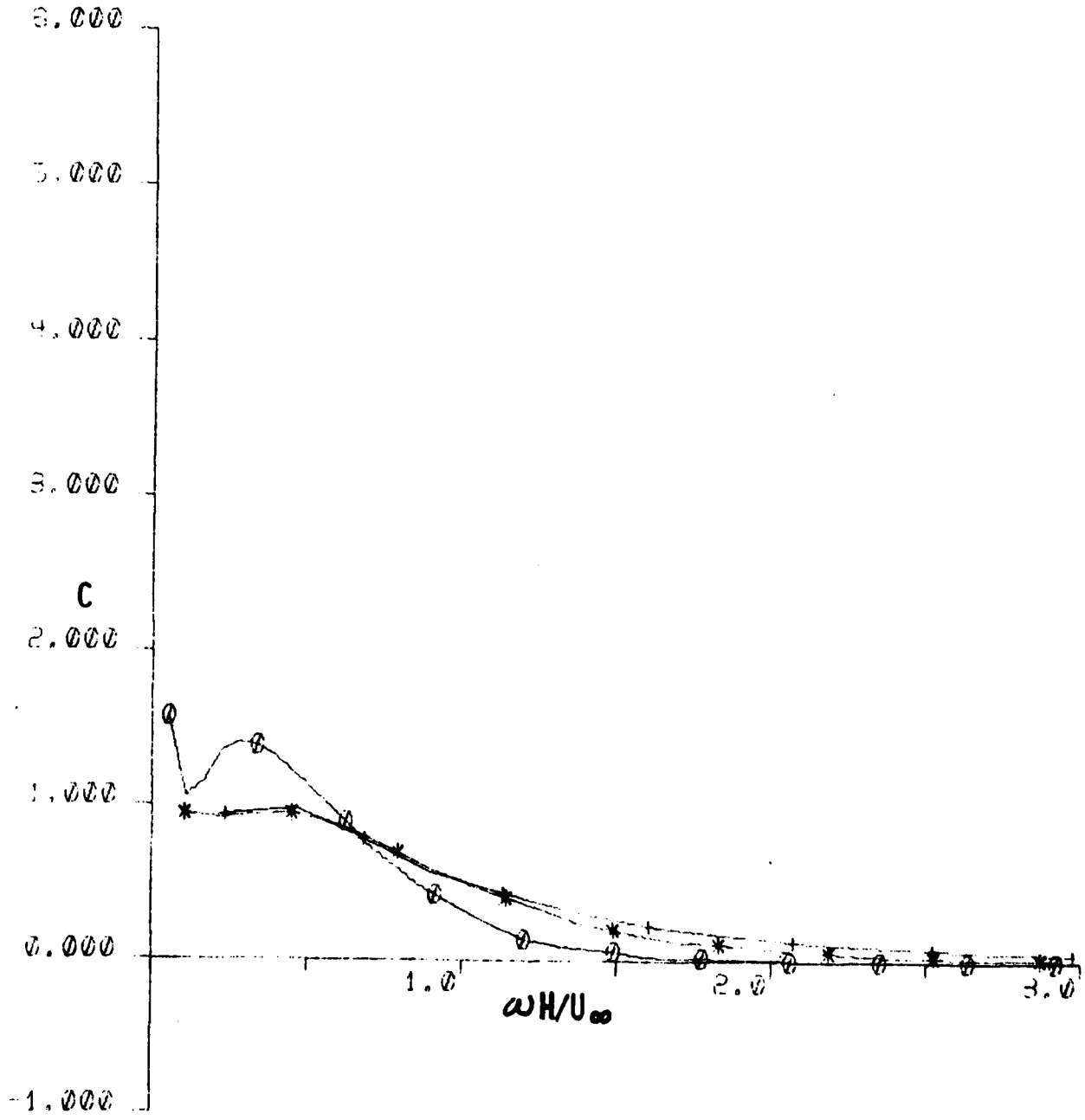

FIGURE 20

Figure 21. Same caption as Fig. 20. Distance downstream of collar is x/H = 16.

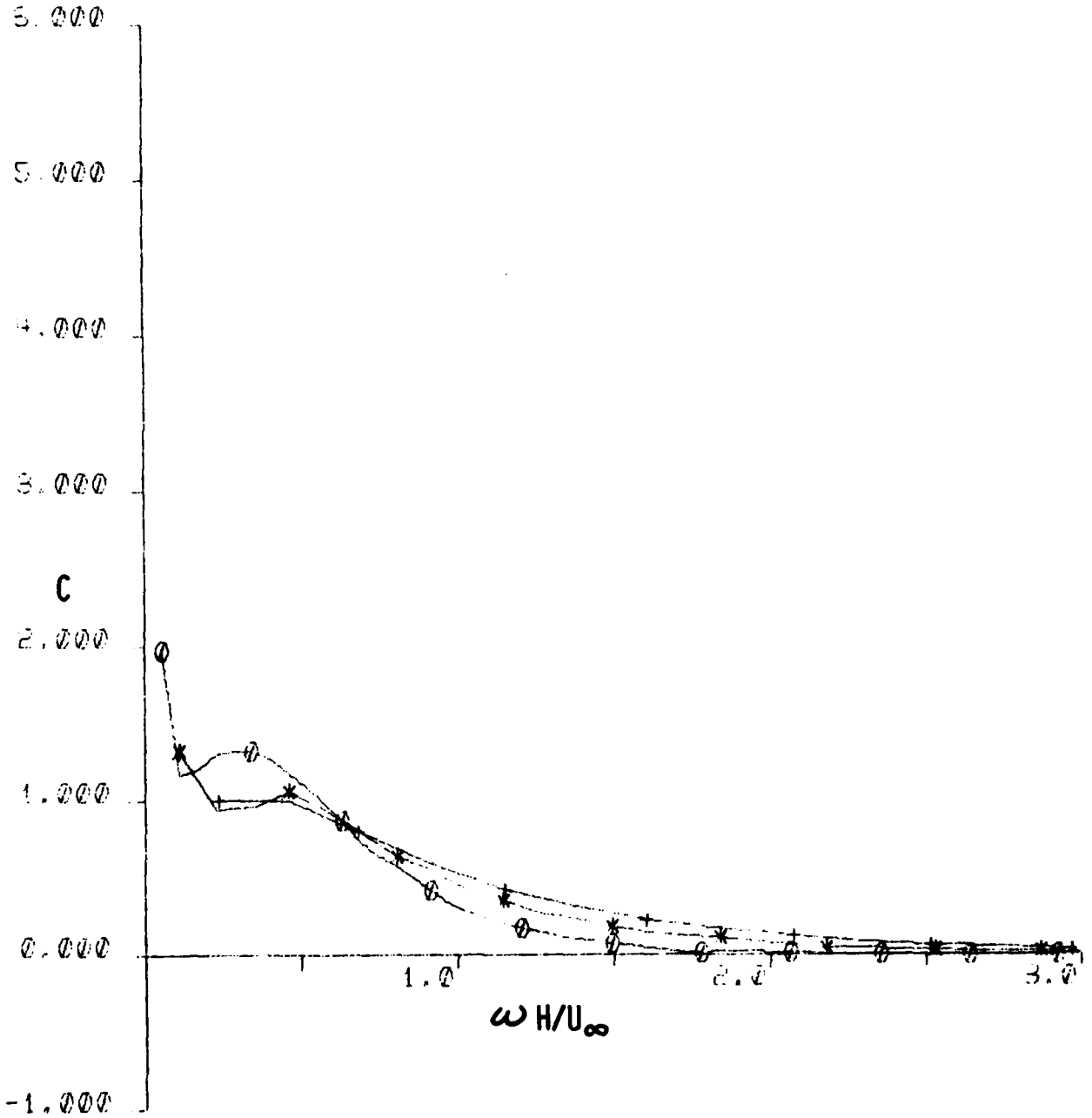

FIGURE 21

Figure 22. Same as Fig. 21 except that x/H = 32.

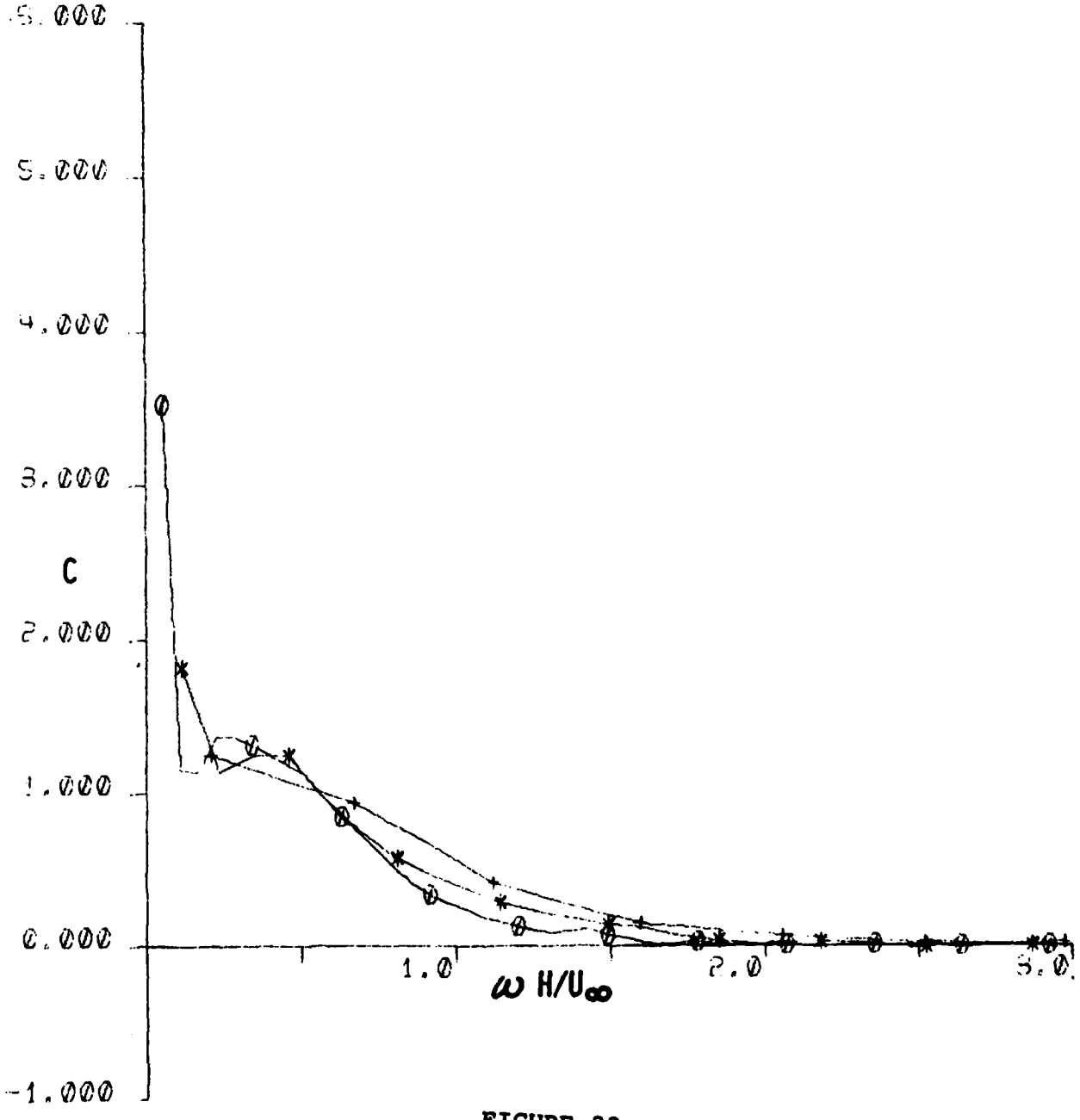

FIGURE 22

Figure 23. Same caption as Fig. 20. +, H/d = 0.25, x/H = 40; *, H/d = 0.125, x/H = 40; ⌀ , H/d = 0.063, x/H = 32.

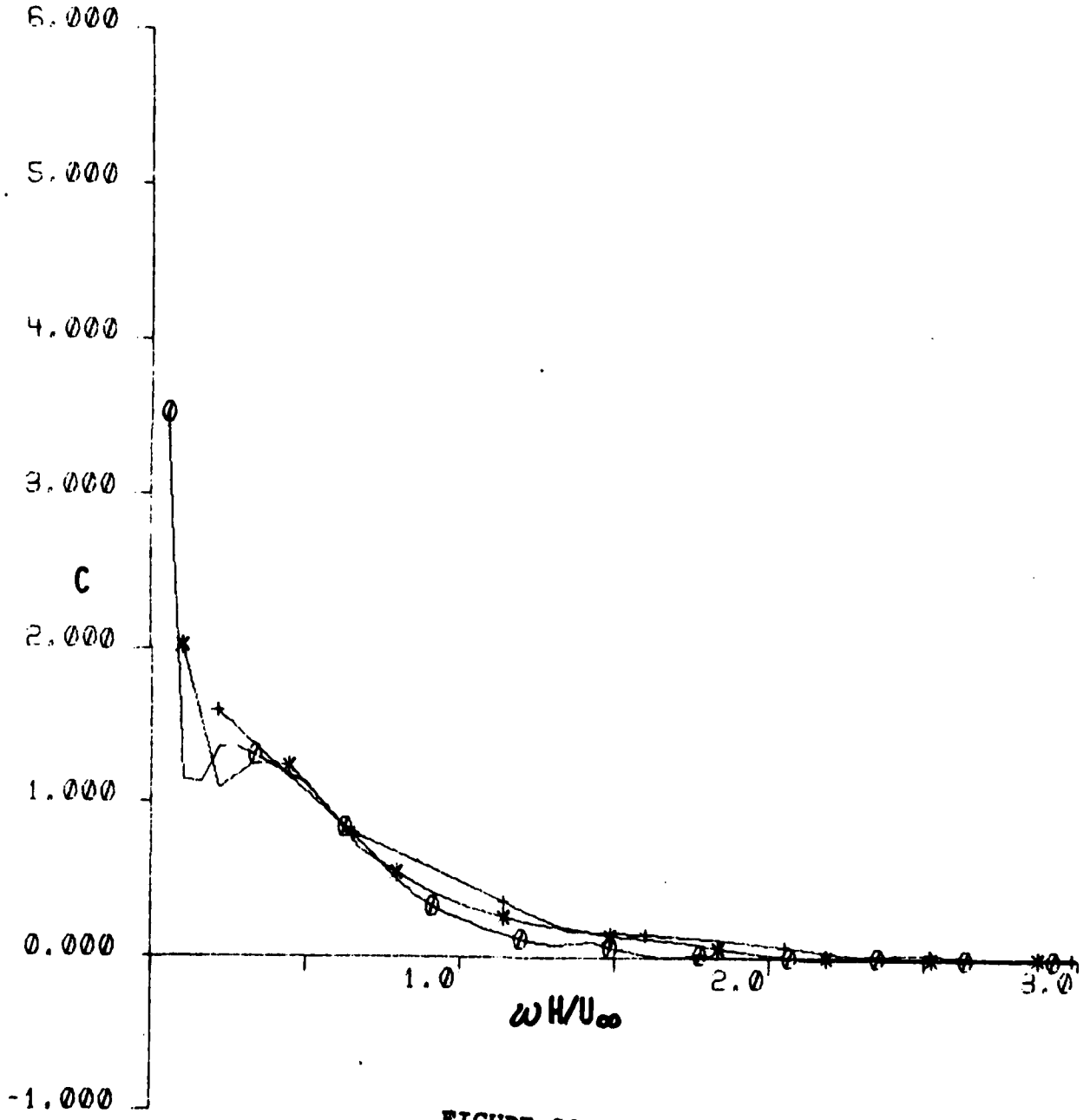

FIGURE 23

Figure 24. Same caption and symbols as Fig. 21 except that x/H = 48.

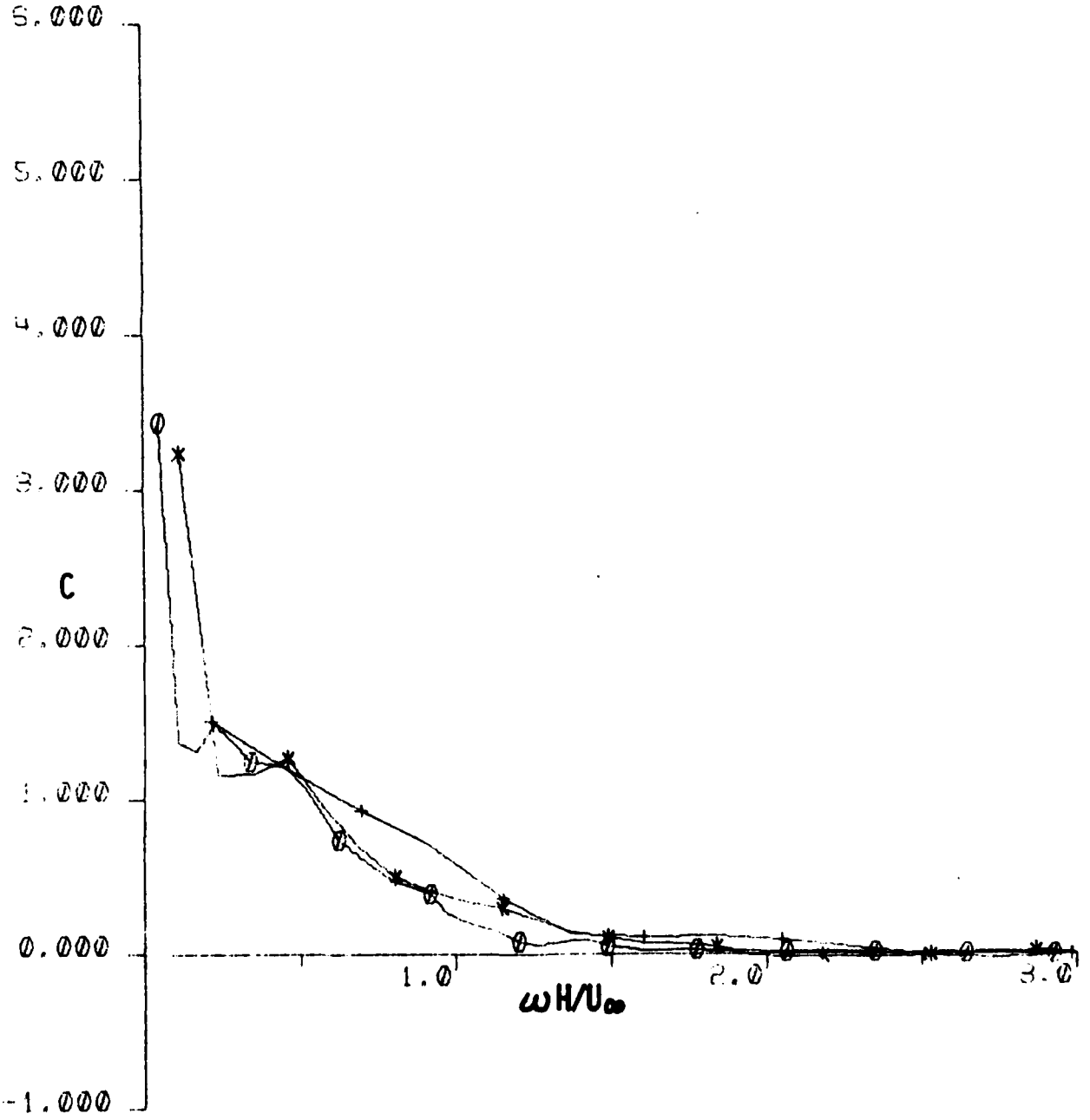

FIGURE 24

Figure 25. Same caption as Fig. 20. +, H/d = 0.25, x/H = 60; *, H/d = 0.125, x/H = 64; Ø , H/d = 0.063, x/H = 64.

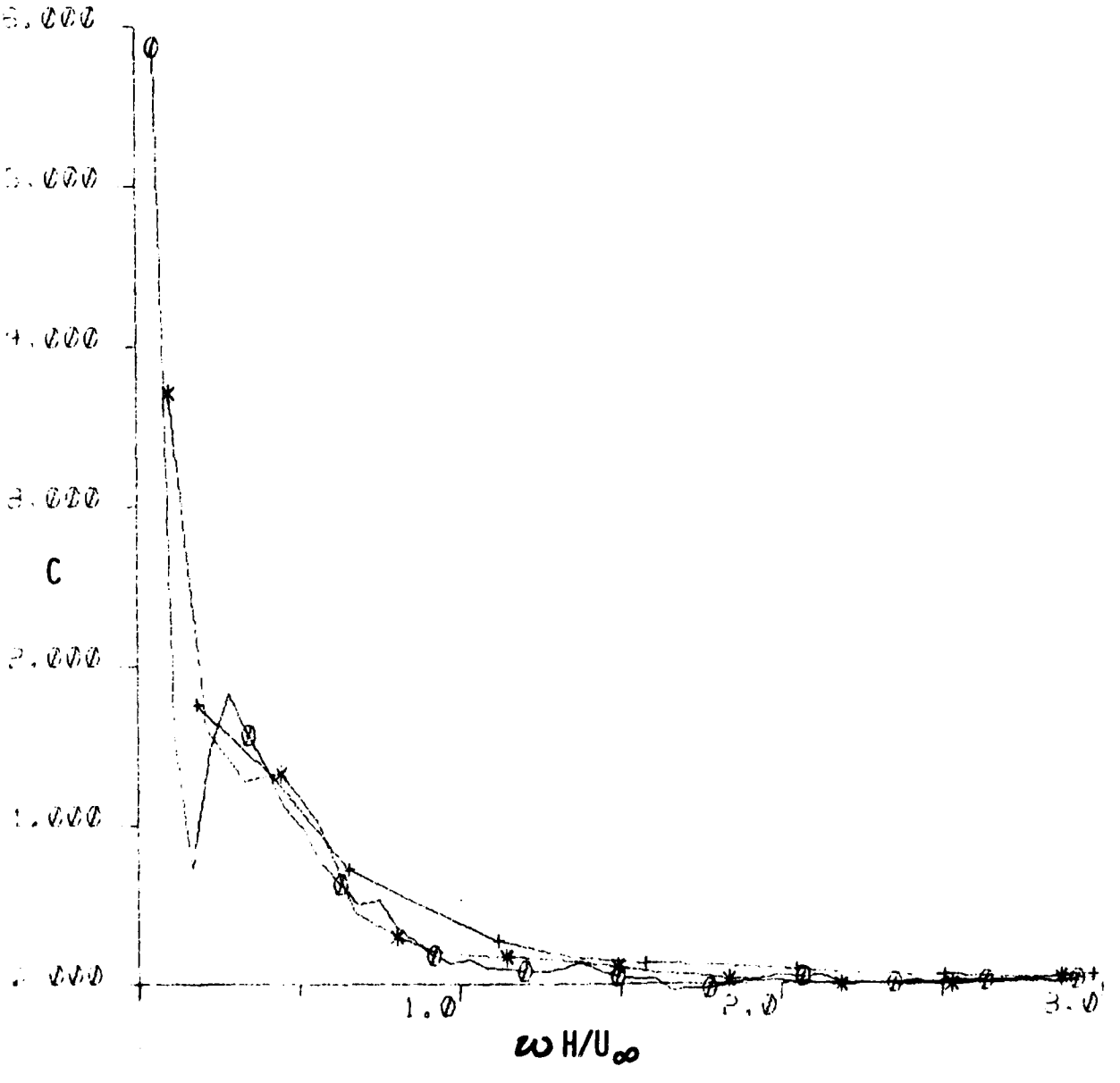

FIGURE 25

Figure 26. Same caption as Fig. 21 except that x/H = 240.

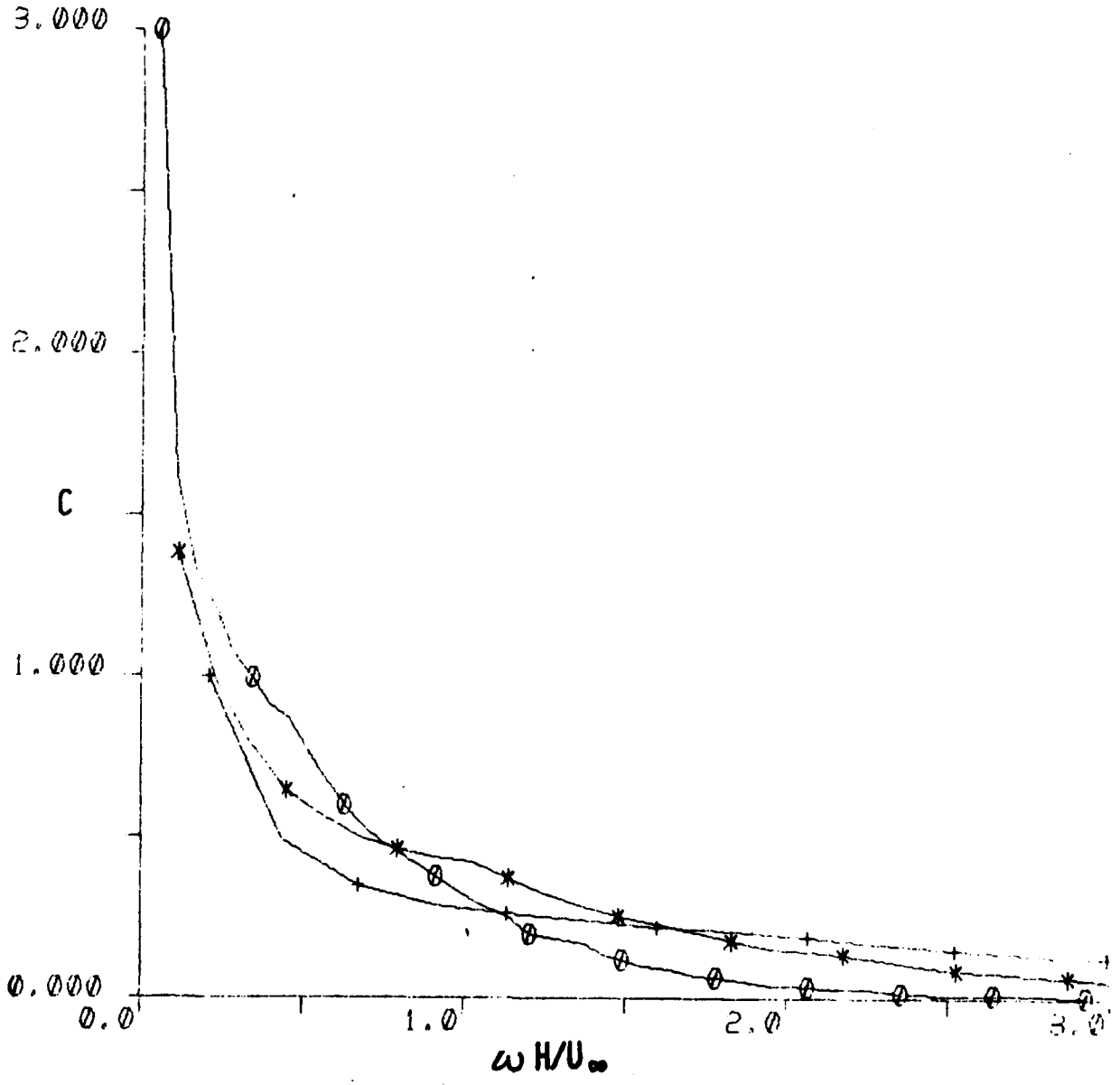

FIGURE 26

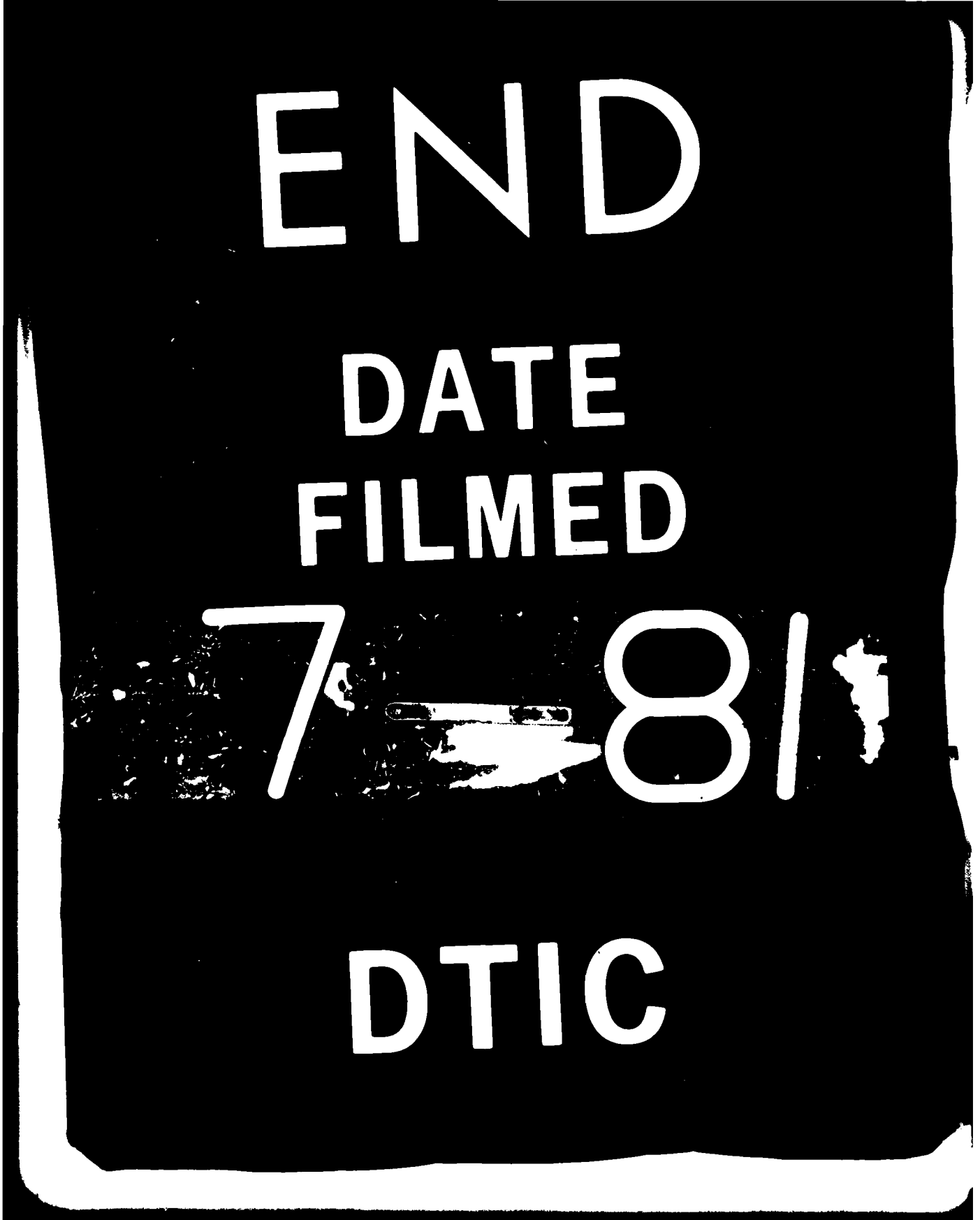
END
DATE
FILMED
7-81
DTIC